

SEARCH FOR GRAVITATIONAL-WAVE BURSTS ASSOCIATED WITH GAMMA-RAY BURSTS USING DATA FROM LIGO SCIENCE RUN 5 AND VIRGO SCIENCE RUN 1

B. P. ABBOTT²⁸, R. ABBOTT²⁸, F. ACERNESE^{18ac}, R. ADHIKARI²⁸, P. AJITH², B. ALLEN^{2,75}, G. ALLEN⁵¹,
M. ALSHOURBAGY^{20ab}, R. S. AMIN³³, S. B. ANDERSON²⁸, W. G. ANDERSON⁷⁵, F. ANTONUCCI^{21a}, S. AOUDIA^{42a},
M. A. ARAIN⁶³, M. ARAYA²⁸, H. ARMANDULA²⁸, P. ARMOR⁷⁵, K. G. ARUN²⁵, Y. ASO²⁸, S. ASTON⁶², P. ASTONE^{21a},
P. AUFMUTH²⁷, C. AULBERT², S. BABAK¹, P. BAKER³⁶, G. BALLARDIN¹¹, S. BALLMER²⁸, C. BARKER²⁹, D. BARKER²⁹,
F. BARONE^{18ac}, B. BARR⁶⁴, P. BARRIGA⁷⁴, L. BARSOTTI³¹, M. BARSUGLIA⁴, M. A. BARTON²⁸, I. BARTOS¹⁰, R. BASSIRI⁶⁴,
M. BASTARRIKA⁶⁴, TH. S. BAUER^{40a}, B. BEHNKE¹, M. BEKER⁴⁰, M. BENACQUISTA⁵⁸, J. BETZWIESER²⁸,
P. T. BEYERSDORF⁴⁷, S. BIGOTTA^{20ab}, I. A. BILENKO³⁷, G. BILLINGSLEY²⁸, S. BIRINDELLI^{42a}, R. BISWAS⁷⁵,
M. A. BIZOUARD²⁵, E. BLACK²⁸, J. K. BLACKBURN²⁸, L. BLACKBURN³¹, D. BLAIR⁷⁴, B. BLAND²⁹, C. BOCCARA¹⁴,
T. P. BODIYA³¹, L. BOGUE³⁰, F. BONDU^{42b}, L. BONELLI^{20ab}, R. BORK²⁸, V. BOSCHI²⁸, S. BOSE⁷⁶, L. BOSI^{19a},
S. BRACCINI^{20a}, C. BRADASCHIA^{20a}, P. R. BRADY⁷⁵, V. B. BRAGINSKY³⁷, J. E. BRAU⁶⁹, D. O. BRIDGES³⁰, A. BRILLET^{42a},
M. BRINKMANN², V. BRISSON²⁵, C. VAN DEN BROECK⁸, A. F. BROOKS²⁸, D. A. BROWN⁵², A. BRUMMIT⁴⁶, G. BRUNET³¹,
R. BUDZYŃSKI^{44b}, T. BULIK^{44cd}, A. BULLINGTON⁵¹, H. J. BULTEN^{40ab}, A. BUONANNO⁶⁵, O. BURMEISTER², D. BUSKULIC²⁶,
R. L. BYER⁵¹, L. CADONATI⁶⁶, G. CAGNOLI^{16a}, E. CALLONI^{18ab}, J. B. CAMP³⁸, E. CAMPAGNA^{16ac}, J. CANNIZZO³⁸,
K. C. CANNON²⁸, B. CANUEL¹¹, J. CAO³¹, F. CARBOGNANI¹¹, L. CARDENAS²⁸, S. CARIDE⁶⁷, G. CASTALDI⁷¹, S. CAUDILL³³,
M. CAVAGLIÀ⁵⁵, F. CAVALIER²⁵, R. CAVALIERI¹¹, G. CELLA^{20a}, C. CEPEDA²⁸, E. CESARINI^{16c}, T. CHALERMSONGSAK²⁸,
E. CHALKLEY⁶⁴, P. CHARLTON⁷⁷, E. CHASSANDE-MOTTIN⁴, S. CHATTERJI²⁸, S. CHELKOWSKI⁶², Y. CHEN^{1,7},
A. CHINCARINI¹⁷, N. CHRISTENSEN⁹, C. T. Y. CHUNG⁵⁴, D. CLARK⁵¹, J. CLARK⁸, J. H. CLAYTON⁷⁵, F. CLEVA^{42a},
E. COCCIA^{22ab}, T. COKELAER⁸, C. N. COLACINO^{13,20}, J. COLAS¹¹, A. COLLA^{21ab}, M. COLOMBINI^{21b}, R. CONTE^{18c},
D. COOK²⁹, T. R. C. CORBITT³¹, C. CORDA^{20ab}, N. CORNISH³⁶, A. CORSI^{21ab}, J.-P. COULON^{42a}, D. COWARD⁷⁴,
D. C. COYNE²⁸, J. D. E. CREIGHTON⁷⁵, T. D. CREIGHTON⁵⁸, A. M. CRUISE⁶², R. M. CULTER⁶², A. CUMMING⁶⁴,
L. CUNNINGHAM⁶⁴, E. CUOCO¹¹, S. L. DANILISHIN³⁷, S. D'ANTONIO^{22a}, K. DANZMANN^{2,27}, A. DARI^{19ab}, V. DATILO¹¹,
B. DAUDERT²⁸, M. DAVIER²⁵, G. DAVIES⁸, E. J. DAW⁵⁶, R. DAY¹¹, R. DE ROSA^{18ab}, D. DEBRA⁵¹, J. DEGALLAIX², M. DEL
PRETE^{20ac}, V. DERGACHEV⁶⁷, S. DESAI⁵³, R. DESALVO²⁸, S. DHURANDHAR²⁴, L. DI FIORE^{18a}, A. DI LIETO^{20ab}, M. DI
PAOLO EMILIO^{22ad}, A. DI VIRGILIO^{20a}, M. DÍAZ⁵⁸, A. DIETZ^{8,26}, F. DONOVAN³¹, K. L. DOOLEY⁶³, E. E. DOOMES⁵⁰,
M. DRAGO^{43cd}, R. W. P. DREVER⁶, J. DUECK², I. DUKE³¹, J.-C. DUMAS⁷⁴, J. G. DWYER¹⁰, C. ECHOLS²⁸, M. EDGAR⁶⁴,
M. EDWARDS⁸, A. EFFLER²⁹, P. EHRENS²⁸, E. ESPINOZA²⁸, T. ETZEL²⁸, M. EVANS³¹, T. EVANS³⁰, V. FAFONE^{22ab},
S. FAIRHURST⁸, Y. FALTAS⁶³, Y. FAN⁷⁴, D. FAZI²⁸, H. FEHRMANN², I. FERRANTE^{20ab}, F. FIDECARO^{20ab}, L. S. FINN⁵³, I.
FIORI¹¹, R. FLAMINIO³², K. FLASCH⁷⁵, S. FOLEY³¹, C. FORREST⁷⁰, N. FOTOPOULOS⁷⁵, J.-D. FOURNIER^{42a}, J. FRANC³²,
A. FRANZEN²⁷, S. FRASCA^{21ab}, F. FRASCONI^{20a}, M. FREDE², M. FREI⁵⁷, Z. FREI¹³, A. FREISE⁶², R. FREY⁶⁹, T. FRICKE³⁰,
P. FRITSCHER³¹, V. V. FROLOV³⁰, M. FYFFE³⁰, V. GALDI⁷¹, L. GAMMAITONI^{19ab}, J. A. GAROFOLI⁵², F. GARUFI^{18ab}, G.
GEMME¹⁷, E. GENIN¹¹, A. GENNAI^{20a}, I. GHOLAMI¹, J. A. GIAIME^{33,30}, S. GIAMPANIS², K. D. GIARDINA³⁰, A.
GIAZOTTO^{20a}, K. GODA³¹, E. GOETZ⁶⁷, L. M. GOGGIN⁷⁵, G. GONZÁLEZ³³, M. L. GORODETSKY³⁷, S. GOESSZETLER⁴⁰,
S. GOSSLER², R. GOUATY³³, M. GRANATA⁴, V. GRANATA²⁶, A. GRANT⁶⁴, S. GRAS⁷⁴, C. GRAY²⁹, M. GRAY⁵,
R. J. S. GREENHALGH⁴⁶, A. M. GREYERSSON¹², C. GREVERIE^{42a}, F. GRIMALDI³¹, R. GROSSO⁵⁸, H. GROTE²,
S. GRUNEWALD¹, M. GUENTHER²⁹, G. GUIDI^{16ac}, E. K. GUSTAFSON²⁸, R. GUSTAFSON⁶⁷, B. HAGE²⁷, J. M. HALLAM⁶²,
D. HAMMER⁷⁵, G. D. HAMMOND⁶⁴, C. HANNA²⁸, J. HANSON³⁰, J. HARMS⁶⁸, G. M. HARRY³¹, I. W. HARRY⁸,
E. D. HARSTAD⁶⁹, K. HAUGHIAN⁶⁴, K. HAYAMA⁵⁸, J. HEEFNER²⁸, H. HEITMANN⁴², P. HELLO²⁵, I. S. HENG⁶⁴,
A. HEPTONSTALL²⁸, M. HEWITSON², S. HILD⁶², E. HIROSE⁵², D. HOAK³⁰, K. A. HODGE²⁸, K. HOLT³⁰, D. J. HOSKEN⁶¹,
J. HOUGH⁶⁴, D. HOYLAND⁷⁴, D. HUET¹¹, B. HUGHEY³¹, S. H. HUTTNER⁶⁴, D. R. INGRAM²⁹, T. ISOGAI⁹, M. ITO⁶⁹,
A. IVANOV²⁸, P. JARANOWSKI^{44e}, B. JOHNSON²⁹, W. W. JOHNSON³³, D. I. JONES⁷², G. JONES⁵, R. JONES⁶⁴,
L. SANCHO DE LA JORDANA⁶⁰, L. JU⁷⁴, P. KALMUS²⁸, V. KALOGERA⁴¹, S. KANDHASAMY⁶⁸, J. KANNER⁶⁵, D. KASPRZYK⁶²,
E. KATSAVOUNIDIS³¹, K. KAWABE²⁹, S. KAWAMURA³⁹, F. KAWAZOE², W. KELLS²⁸, D. G. KEPPEL²⁸, A. KHALAIDOVSKI²,
F. Y. KHALILI³⁷, R. KHAN¹⁰, E. KHAZANOV²³, P. KING²⁸, J. S. KISSEL³³, S. KLIMENKO⁶³, K. KOKEYAMA³⁹,
V. KONDRASHOV²⁸, R. KOPPARAPU⁵³, S. KORANDA⁷⁵, I. KOWALSKA^{44c}, D. KOZAK²⁸, B. KRISHNAN¹, A. KRÓLAK^{44af},
R. KUMAR⁶⁴, P. KWEE²⁷, P. LA PENNA¹¹, P. K. LAM⁵, M. LANDRY²⁹, B. LANTZ⁵¹, A. LAZZARINI²⁸, H. LEI⁵⁸, M. LEI²⁸,
N. LEINDECKER⁵¹, I. LEONOR⁶⁹, N. LEROY²⁵, N. LETENDRE²⁶, C. LI⁷, H. LIN⁶³, P. E. LINDQUIST²⁸, T. B. LITTENBERG³⁶,
N. A. LOCKERBIE⁷³, D. LODHIA⁶², M. LONGO⁷¹, M. LORENZINI^{16a}, V. LORLETTE¹⁴, M. LORMAND³⁰, G. LOSURDO^{16a},
P. LU⁵¹, M. LUBINSKI²⁹, A. LUCIANETTI⁶³, H. LÜCK^{2,27}, B. MACHENSCHALK¹, M. MACINNIS³¹, J.-M. MACKOWSKI³²,
M. MAGESWARAN²⁸, K. MAILAND²⁸, E. MAJORANA^{21a}, N. MAN^{42a}, I. MANDEL⁴¹, V. MANDIC⁶⁸, M. MANTOVANI^{20c},
F. MARCHESONI^{19a}, F. MARION²⁶, S. MÁRKA¹⁰, Z. MÁRKA¹⁰, A. MARKOSYAN⁵¹, J. MARKOWITZ³¹, E. MAROS²⁸, J.
MARQUE¹¹, F. MARTELLI^{16ac}, I. W. MARTIN⁶⁴, R. M. MARTIN⁶³, J. N. MARX²⁸, K. MASON³¹, A. MASSEROT²⁶,
F. MATICHARD³³, L. MATONE¹⁰, R. A. MATZNER⁵⁷, N. MAVALVALA³¹, R. MCCARTHY²⁹, D. E. MCCLELLAND⁵,
S. C. MCGUIRE⁵⁰, M. MCHUGH³⁵, G. MCINTYRE²⁸, D. J. A. MCKECHAN⁸, K. MCKENZIE⁵, M. MEHMET², A. MELATOS⁵⁴,
A. C. MELISSINOS⁷⁰, G. MENDELL²⁹, D. F. MENÉNDEZ⁵³, F. MENZINGER¹¹, R. A. MERCER⁷⁵, S. MESHKOV²⁸,
C. MESSENGER², M. S. MEYER³⁰, C. MICHEL³², L. MILANO^{18ab}, J. MILLER⁶⁴, J. MINELLI⁵³, Y. MINENKOV⁵⁸, Y. MINO⁷,
V. P. MITROFANOV³⁷, G. MITSSELMAKER⁶³, R. MITTLEMAN³¹, O. MIYAKAWA²⁸, B. MOE⁷⁵, M. MOHAN¹¹,
S. D. MOHANTY⁵⁸, S. R. P. MOHAPATRA⁶⁶, J. MOREAU¹⁴, G. MORENO²⁹, N. MORGADO³², A. MORGIA^{22ab}, T. MORIOKA³⁹,
K. MORS², S. MOSCA^{18ab}, V. MOSCATELLI^{21a}, K. MOSSAVI², B. MOURS²⁶, C. MOWLOWRY⁵, G. MUELLER⁶³,
D. MUHAMMAD³⁰, H. ZUR MÜHLEN²⁷, S. MUKHERJEE⁵⁸, H. MUKHOPADHYAY²⁴, A. MULLAVEY⁵, H. MÜLLER-EBHARDT²,
J. MUNCH⁶¹, P. G. MURRAY⁶⁴, E. MYERS²⁹, J. MYERS²⁹, T. NASH²⁸, J. NELSON⁶⁴, I. NERI^{19ab}, G. NEWTON⁶⁴,

A. NISHIZAWA³⁹, F. NOCERA¹¹, K. NUMATA³⁸, E. OCHSNER⁶⁵, J. O'DELL⁴⁶, G. H. OGIN²⁸, B. O'REILLY³⁰,
R. O'SHAUGHNESSY⁵³, D. J. OTTAWAY⁶¹, R. S. OTTENS⁶³, H. OVERMIER³⁰, B. J. OWEN⁵³, G. PAGLIAROLI^{22ad}, C.
PALOMBA^{21a}, Y. PAN⁶⁵, C. PANKOW⁶³, F. PAOLETTI^{20a,11}, M. A. PAPA^{1,75}, V. PARAMESHWARAIAH²⁹, S. PARDI^{18ab}, A.
PASQUALETTI¹¹, R. PASSAQUIETI^{20ab}, D. PASSUELLO^{20a}, P. PATEL²⁸, M. PEDRAZA²⁸, S. PENN¹⁵, A. PERRECA⁶², G.
PERSICHETTI^{18ab}, M. PICHOT^{42a}, F. PIERGIOVANNI^{16ac}, V. PIERRO⁷¹, M. PIETKA^{44e}, L. PINARD³², I. M. PINTO⁷¹,
M. PITKIN⁶⁴, H. J. PLETSCHE², M. V. PLISSI⁶⁴, R. POGGIANI^{20ab}, F. POSTIGLIONE^{18c}, M. PRATO¹⁷, M. PRINCIPE⁷¹,
R. PRIX², G.A. PRODI^{43ab}, L. PROKHOROV³⁷, O. PUNKEN², M. PUNTURO^{19a}, P. PUPPO^{21a}, V. QUETSCHKE⁶³,
F. J. RAAB²⁹, O. RABASTE⁴, D. S. RABELING^{40ab}, H. RADKINS²⁹, P. RAFFAI¹³, Z. RAICS¹⁰, N. RAINER²,
M. RAKHMANOV⁵⁸, P. RAPAGNANI^{21ab}, V. RAYMOND⁴¹, V. RE^{43ab}, C. M. REED²⁹, T. REED³⁴, T. REGIMBAU^{42a},
H. REHBEIN², S. REID⁶⁴, D. H. REITZE⁶³, F. RICCI^{21ab}, R. RIESEN³⁰, K. RILES⁶⁷, B. RIVERA²⁹, P. ROBERTS³,
N. A. ROBERTSON^{28,64}, F. ROBINET²⁵, C. ROBINSON⁸, E. L. ROBINSON¹, A. ROCCHI^{22a}, S. RODDY³⁰, L. ROLLAND²⁶,
J. ROLLINS¹⁰, J. D. ROMANO⁵⁸, R. ROMANO^{18ac}, J. H. ROMIE³⁰, D. ROSIŃSKA^{44gd}, C. RÖVER², S. ROWAN⁶⁴, A. RÜDIGER²,
P. RUGGI¹¹, P. RUSSELL²⁸, K. RYAN²⁹, S. SAKATA³⁹, F. SALEMI^{43ab}, V. SANDBERG²⁹, V. SANNIBALE²⁸, L. SANTAMARÍA¹,
S. SARAF⁴⁸, P. SARIN³¹, B. SASSOLAS³², B. S. SATHYAPRAKASH⁸, S. SATO³⁹, M. SATTERTHWAITE⁵, P. R. SAULSON⁵²,
R. SAVAGE²⁹, P. SAVOV⁷, M. SCANLAN³⁴, R. SCHILLING², R. SCHNABEL², R. SCHOFIELD⁶⁹, B. SCHULZ², B. F. SCHUTZ^{1,8},
P. SCHWINBERG²⁹, J. SCOTT⁶⁴, S. M. SCOTT⁵, A. C. SEARLE²⁸, B. SEARS²⁸, F. SEIFERT², D. SELLERS³⁰,
A. S. SENGUPTA²⁸, D. SENTENAC¹¹, A. SERGEEV²³, B. SHAPIRO³¹, P. SHAWHAN⁶⁵, D. H. SHOEMAKER³¹, A. SIBLEY³⁰,
X. SIEMENS⁷⁵, D. SIGG²⁹, S. SINHA⁵¹, A. M. SINTES⁶⁰, B. J. J. SLAGMOLEN⁵, J. SLUTSKY³³, M. V. VAN DER SLUYS⁴¹,
J. R. SMITH⁵², M. R. SMITH²⁸, N. D. SMITH³¹, K. SOMIYA⁷, B. SORAZU⁶⁴, A. STEIN³¹, L. C. STEIN³¹, S. STEPLEWSKI⁷⁶,
A. STOCHINO²⁸, R. STONE⁵⁸, K. A. STRAIN⁶⁴, S. STRIGIN³⁷, A. STROEER³⁸, R. STURANI^{16ac}, A. L. STUVER³⁰,
T. Z. SUMMERSCALES³, K. -X. SUN⁵¹, M. SUNG³³, P. J. SUTTON⁸, B. SWINKELS¹¹, G. P. SZOKOLY¹³, D. TALUKDER⁷⁶,
L. TANG⁵⁸, D. B. TANNER⁶³, S. P. TARABRIN³⁷, J. R. TAYLOR², R. TAYLOR²⁸, R. TERENCE^{22ac}, J. THACKER³⁰,
K. A. THORNE³⁰, K. S. THORNE⁷, A. THÜRING²⁷, K. V. TOKMAKOV⁶⁴, A. TONCELLI^{20ab}, M. TONELLI^{20ab}, C. TORRES³⁰,
C. TORRIE²⁸, E. TOURNEFIER²⁶, F. TRAVASSO^{19ab}, G. TRAYLOR³⁰, M. TRIAS⁶⁰, J. TRUMMER²⁶, D. UGOLINI⁵⁹, J. ULMEN⁵¹,
K. URBANEK⁵¹, H. VAHLBRUCH²⁷, G. VAJENTE^{20ab}, M. VALLISNERI⁷, J.F.J. VAN DEN BRAND^{40ab}, S. VAN DER PUTTEN^{40a},
S. VASS²⁸, R. VAULIN⁷⁵, M. VAVOULIDIS²⁵, A. VECCHIO⁶², G. VEDOVATO^{43c}, A. A. VAN VEGGEL⁶⁴, J. VEITCH⁶²,
P. VEITCH⁶¹, C. VELTKAMP², D. VERKINDT²⁶, F. VETRANO^{16ac}, A. VICERÉ^{16ac}, A. VILLAR²⁸, J.-Y. VINET^{42a}, H.
VOCCA^{19a}, C. VORVICK²⁹, S. P. VYACHANIN³⁷, S. J. WALDMAN³¹, L. WALLACE²⁸, R. L. WARD²⁸, M. WAS²⁵,
A. WEIDNER², M. WEINERT², A. J. WEINSTEIN²⁸, R. WEISS³¹, L. WEN^{7,74}, S. WEN³³, K. WETTE⁵, J. T. WHELAN^{1,45},
S. E. WHITCOMB²⁸, B. F. WHITING⁶³, C. WILKINSON²⁹, P. A. WILLEMS²⁸, H. R. WILLIAMS⁵³, L. WILLIAMS⁶³,
B. WILLKE^{2,27}, I. WILMUT⁴⁶, L. WINKELMANN², W. WINKLER², C. C. WIPF³¹, A. G. WISEMAN⁷⁵, G. WOAN⁶⁴,
R. WOOLEY³⁰, J. WORDEN²⁹, W. WU⁶³, I. YAKUSHIN³⁰, H. YAMAMOTO²⁸, Z. YAN⁷⁴, S. YOSHIDA⁴⁹, M. YVERT²⁶,
M. ZANOLIN¹², J. ZHANG⁶⁷, L. ZHANG²⁸, C. ZHAO⁷⁴, N. ZOTOV³⁴, M. E. ZUCKER³¹, J. ZWEIZIG²⁸

¹Albert-Einstein-Institut, Max-Planck-Institut für Gravitationsphysik, D-14476 Golm, Germany

²Albert-Einstein-Institut, Max-Planck-Institut für Gravitationsphysik, D-30167 Hannover, Germany

³Andrews University, Berrien Springs, MI 49104 USA

⁴AstroParticule et Cosmologie (APC), CNRS: UMR7164-IN2P3-Observatoire de Paris-Université Denis Diderot-Paris VII - CEA : DSM/IRFU

⁵Australian National University, Canberra, 0200, Australia

⁶California Institute of Technology, Pasadena, CA 91125, USA

⁷Caltech-CaRT, Pasadena, CA 91125, USA

⁸Cardiff University, Cardiff, CF24 3AA, United Kingdom

⁹Carleton College, Northfield, MN 55057, USA

⁷⁷Charles Sturt University, Wagga Wagga, NSW 2678, Australia

¹⁰Columbia University, New York, NY 10027, USA

¹¹European Gravitational Observatory (EGO), I-56021 Cascina (Pi), Italy

¹²Embry-Riddle Aeronautical University, Prescott, AZ 86301 USA

¹³Eötvös University, ELTE 1053 Budapest, Hungary

¹⁴ESPCI, CNRS, F-75005 Paris, France

¹⁵Hobart and William Smith Colleges, Geneva, NY 14456, USA

¹⁶INFN, Sezione di Firenze, I-50019 Sesto Fiorentino^a; Università degli Studi di Firenze, I-50121^b, Firenze; Università degli Studi di Urbino 'Carlo Bo', I-61029 Urbino^c, Italy

¹⁷INFN, Sezione di Genova; I-16146 Genova, Italy

¹⁸INFN, sezione di Napoli ^a; Università di Napoli 'Federico II'^b Complesso Universitario di Monte S. Angelo, I-80126 Napoli; Università di Salerno, Fisciano, I-84084 Salerno^c, Italy

¹⁹INFN, Sezione di Perugia^a; Università di Perugia^b, I-6123 Perugia, Italy

²⁰INFN, Sezione di Pisa^a; Università di Pisa^b; I-56127 Pisa; Università di Siena, I-53100 Siena^c, Italy

²¹INFN, Sezione di Roma^a; Università 'La Sapienza'^b, I-00185 Roma, Italy

²²INFN, Sezione di Roma Tor Vergata^a; Università di Roma Tor Vergata^b, Istituto di Fisica dello Spazio Interplanetario (IFSI) INAF^c, I-00133 Roma; Università dell'Aquila, I-67100 L'Aquila^d, Italy

²³Institute of Applied Physics, Nizhny Novgorod, 603950, Russia

²⁴Inter-University Centre for Astronomy and Astrophysics, Pune - 411007, India

²⁵LAL, Université Paris-Sud, IN2P3/CNRS, F-91898 Orsay, France

²⁶Laboratoire d'Annecy-le-Vieux de Physique des Particules (LAPP), IN2P3/CNRS, Université de Savoie, F-74941 Annecy-le-Vieux, France

²⁷Leibniz Universität Hannover, D-30167 Hannover, Germany

²⁸LIGO - California Institute of Technology, Pasadena, CA 91125, USA

²⁹LIGO - Hanford Observatory, Richland, WA 99352, USA

³⁰LIGO - Livingston Observatory, Livingston, LA 70754, USA

³¹LIGO - Massachusetts Institute of Technology, Cambridge, MA 02139, USA

³²Laboratoire des Matériaux Avancés (LMA), IN2P3/CNRS, F-69622 Villeurbanne, Lyon, France

- ³³Louisiana State University, Baton Rouge, LA 70803, USA
³⁴Louisiana Tech University, Ruston, LA 71272, USA
³⁵Loyola University, New Orleans, LA 70118, USA
³⁶Montana State University, Bozeman, MT 59717, USA
³⁷Moscow State University, Moscow, 119992, Russia
³⁸NASA/Goddard Space Flight Center, Greenbelt, MD 20771, USA
³⁹National Astronomical Observatory of Japan, Tokyo 181-8588, Japan
⁴⁰Nikhef, National Institute for Subatomic Physics, P.O. Box 41882, 1009 DB Amsterdam, The Netherlands^a; VU University Amsterdam, De Boelelaan 1081, 1081 HV Amsterdam, The Netherlands^b
⁴¹Northwestern University, Evanston, IL 60208, USA
⁴²Departement Artemis, Observatoire de la Côte d'Azur, CNRS, F-06304 Nice ^a; Institut de Physique de Rennes, CNRS, Université de Rennes 1, 35042 Rennes ^b; France
⁴³INFN, Gruppo Collegato di Trento^a and Università di Trento^b, I-38050 Povo, Trento, Italy; INFN, Sezione di Padova^c and Università di Padova^d, I-35131 Padova, Italy
⁴⁴IM-PAN 00-956 Warsaw^a; Warsaw Univ. 00-681^b; Astro. Obs. Warsaw Univ. 00-478^c; CAMK-PAM 00-716 Warsaw^d; Białystok Univ. 15-424^e; IPJ 05-400 Swierk-Otwock^f; Inst. of Astronomy 65-265 Zielona Góra ^g, Poland
⁴⁵Rochester Institute of Technology, Rochester, NY 14623, USA
⁴⁶Rutherford Appleton Laboratory, HSIC, Chilton, Didcot, Oxon OX11 0QX United Kingdom
⁴⁷San Jose State University, San Jose, CA 95192, USA
⁴⁸Sonoma State University, Rohnert Park, CA 94928, USA
⁴⁹Southeastern Louisiana University, Hammond, LA 70402, USA
⁵⁰Southern University and A&M College, Baton Rouge, LA 70813, USA
⁵¹Stanford University, Stanford, CA 94305, USA
⁵²Syracuse University, Syracuse, NY 13244, USA
⁵³The Pennsylvania State University, University Park, PA 16802, USA
⁵⁴The University of Melbourne, Parkville VIC 3010, Australia
⁵⁵The University of Mississippi, University, MS 38677, USA
⁵⁶The University of Sheffield, Sheffield S10 2TN, United Kingdom
⁵⁷The University of Texas at Austin, Austin, TX 78712, USA
⁵⁸The University of Texas at Brownsville and Texas Southmost College, Brownsville, TX 78520, USA
⁵⁹Trinity University, San Antonio, TX 78212, USA
⁶⁰Universitat de les Illes Balears, E-07122 Palma de Mallorca, Spain
⁶¹University of Adelaide, Adelaide, SA 5005, Australia
⁶²University of Birmingham, Birmingham, B15 2TT, United Kingdom
⁶³University of Florida, Gainesville, FL 32611, USA
⁶⁴University of Glasgow, Glasgow, G12 8QQ, United Kingdom
⁶⁵University of Maryland, College Park, MD 20742 USA
⁶⁶University of Massachusetts - Amherst, Amherst, MA 01003, USA
⁶⁷University of Michigan, Ann Arbor, MI 48109, USA
⁶⁸University of Minnesota, Minneapolis, MN 55455, USA
⁶⁹University of Oregon, Eugene, OR 97403, USA
⁷⁰University of Rochester, Rochester, NY 14627, USA
⁷¹University of Sannio at Benevento, I-82100 Benevento, Italy
⁷²University of Southampton, Southampton, SO17 1BJ, United Kingdom
⁷³University of Strathclyde, Glasgow, G1 1XQ, United Kingdom
⁷⁴University of Western Australia, Crawley, WA 6009, Australia
⁷⁵University of Wisconsin-Milwaukee, Milwaukee, WI 53201, USA and
⁷⁶Washington State University, Pullman, WA 99164, USA

Draft version June 5, 2022

ABSTRACT

We present the results of a search for gravitational-wave bursts associated with 137 gamma-ray bursts (GRBs) that were detected by satellite-based gamma-ray experiments during the fifth LIGO science run and first Virgo science run. The data used in this analysis were collected from 2005 November 4 to 2007 October 1, and most of the GRB triggers were from the *Swift* satellite. The search uses a coherent network analysis method that takes into account the different locations and orientations of the interferometers at the three LIGO-Virgo sites. We find no evidence for gravitational-wave burst signals associated with this sample of GRBs. Using simulated short-duration (< 1 s) waveforms, we set upper limits on the amplitude of gravitational waves associated with each GRB. We also place lower bounds on the distance to each GRB under the assumption of a fixed energy emission in gravitational waves, with typical limits of $D \sim 15$ Mpc ($E_{\text{GW}}^{\text{iso}}/0.01M_{\odot}c^2$)^{1/2} for emission at frequencies around 150 Hz, where the LIGO-Virgo detector network has best sensitivity. We present astrophysical interpretations and implications of these results, and prospects for corresponding searches during future LIGO-Virgo runs.

Subject headings: gamma-ray bursts – gravitational waves – compact object mergers – soft gamma-ray repeaters

1. INTRODUCTION

Gamma-ray bursts (GRBs) are intense flashes of γ -rays which occur approximately once per day and are isotropically distributed over the sky (see, e.g.: Mészáros 2006,

and references therein). The variability of the bursts on time scales as short as a millisecond indicates that the sources are very compact, while the identification of host galaxies and the measurement of redshifts for more than

100 bursts have shown that GRBs are of extra-galactic origin.

GRBs are grouped into two broad classes by their characteristic duration and spectral hardness (Kouveliotou et al. 1993; Gehrels et al. 2006). The progenitors of most short GRBs ($\lesssim 2$ s, with hard spectra) are widely thought to be mergers of neutron star binaries or neutron star-black hole binaries; see Nakar (2007) and references therein. A small fraction (up to $\simeq 15\%$) of short-duration GRBs are also thought to be due to giant flares from a local distribution of soft-gamma repeaters (SGRs) (Duncan & Thompson 1992; Nakar et al. 2006; Chapman et al. 2008). Long GRBs ($\gtrsim 2$ s, with soft spectra), on the other hand, are associated with core-collapse supernovae (Galama et al. 1998; Hjorth et al. 2003; Malesani et al. 2004; Campana et al. 2006). Both the merger and supernova scenarios result in the formation of a stellar-mass black hole with accretion disk (Fryer et al. 1999; Cannizzo & Gehrels 2009), and the emission of gravitational radiation is expected in this process.

To date, several searches for gravitational-wave bursts (GWBs) associated with gamma-ray bursts (GRBs) have been performed using data from LIGO or Virgo. Data from the second LIGO science run were used to search for a gravitational-wave signal from GRB 030329/SN 2003dh (Abbott et al. 2005), a bright GRB and associated supernova located at a redshift of $z = 0.1685$. This was followed by a search for GWBs coincident with 39 GRBs which were detected during the second, third, and fourth LIGO science runs (Abbott et al. 2008b). Data from the Virgo detector were used to search for a GWB associated with GRB 050915a (Acernese et al. 2007, 2008a). Most recently, data from the fifth LIGO science run was analyzed to search for a GWB or binary coalescence inspiral signal from GRB 070201 (Abbott et al. 2008a). This short-duration GRB had a position error box overlapping the Andromeda galaxy (M31), located at a distance of 770 kpc. No evidence for a gravitational-wave signal was found in these searches. In the case of GRB 070201, the non-detection of associated gravitational waves provided important information about its progenitor, ruling out a compact-object binary in M31 with high confidence.

In this paper, we present the results of a search for gravitational-wave bursts associated with 137 GRBs that were detected by satellite-based gamma-ray experiments during the fifth LIGO science run (S5) and first Virgo science run (VSR1), which collectively spanned the period from 2005 November 4 to 2007 October 1. This is the first joint search for gravitational waves by LIGO and Virgo; it also uses improved methods compared to previous searches, and is thus able to achieve better sensitivity.

We search for GWBs from both short- and long-duration GRBs. Since the precise nature of the radiation depends on the somewhat-unknown progenitor model, and we analyse both short and long GRBs, the search methods presented in this paper do not require specific knowledge of the gravitational waveforms. Instead, we look for unmodelled burst signals with duration $\lesssim 1$ s and frequencies in the LIGO/Virgo band, approximately 60 Hz – 2000 Hz. The results of a template-based search specifically targeting binary inspiral gravitational-wave signals associated with short GRBs will be presented separately (Abbott et al. 2009c).

Although it is expected that most GRB progenitors will be at distances too large for the resulting gravitational-wave signals to be detectable by LIGO and Virgo (Berger et al. 2005), it is possible that a few GRBs could be located nearby. For example, the smallest observed redshift of an optical GRB afterglow is $z = 0.0085$ ($\simeq 36$ Mpc), for GRB 980425 (Kulkarni et al. 1998; Galama et al. 1998; Iwamoto et al. 1998); this would be within the LIGO-Virgo detectable range for some progenitor models. Recent studies (Liang et al. 2007; Chapman et al. 2007) indicate the existence of a local population of under-luminous long GRBs with an observed rate density (number per unit volume per unit time) approximately 10^3 times that of the high-luminosity population. Also, observations seem to suggest that short-duration GRBs tend to have smaller redshifts than long GRBs (Guetta & Piran 2005; Fox et al. 2005), and this has led to fairly optimistic estimates (Nakar et al. 2006; Guetta & Piran 2006) for detecting associated gravitational-wave emission in an extended LIGO science run. Approximately 70% of the GRBs in our sample do not have measured redshifts, so it is possible that one or more could be much closer than the typical Gpc distance of GRBs.

The paper is organized as follows. Section 2 describes the LIGO and Virgo detectors, and Sec. 3 describes the GRB sample during LIGO Science Run 5 / Virgo Science Run 1. We summarize the analysis procedure in Sec. 4. Two independent analysis “pipelines” are used to search for GWBs. Section 5 details the results of the search. No significant signal is found in association with any of the 137 GRBs studied. A statistical analysis of the collective GRB sample also shows no sign of a collective signature of weak GWBs. In Sec. 6 we place upper limits on the amplitude of gravitational waves associated with each GRB. We also set lower limits on the distance to each GRB assuming a fixed energy emission in gravitational waves. We conclude in Sec. 7 with some comments on the astrophysical significance of these results and the prospects for future GRB searches.

2. LIGO SCIENCE RUN 5 & VIRGO SCIENCE RUN 1

The LIGO detectors are kilometer-scale power-recycled Michelson interferometers with orthogonal Fabry-Perot arms (Abbott et al. 2004, 2009a). They are designed to detect gravitational waves with frequencies ranging from ~ 40 Hz to several kHz. The interferometers’ maximum sensitivity occurs near 150 Hz. There are two LIGO observatories: one located at Hanford, WA and the other at Livingston, LA. The Hanford site houses two interferometers: one with 4 km arms (H1), and the other with 2 km arms (H2). The Livingston observatory has one 4 km interferometer (L1). The observatories are separated by a distance of 3000 km, corresponding to a time-of-flight separation of 10 ms.

The Virgo detector (V1) is in Cascina near Pisa, Italy. It is a 3 km long power-recycled Michelson interferometer with orthogonal Fabry-Perot arms (Acernese et al. 2008b). During VSR1, the Virgo detector had sensitivity similar to the LIGO 4 km interferometers above approximately 500 Hz. The time-of-flight separation between the Virgo and Hanford observatories is 27 ms, and between Virgo and Livingston it is 25 ms.

A gravitational wave is a spacetime metric perturbation that is manifested as a time-varying quadrupolar

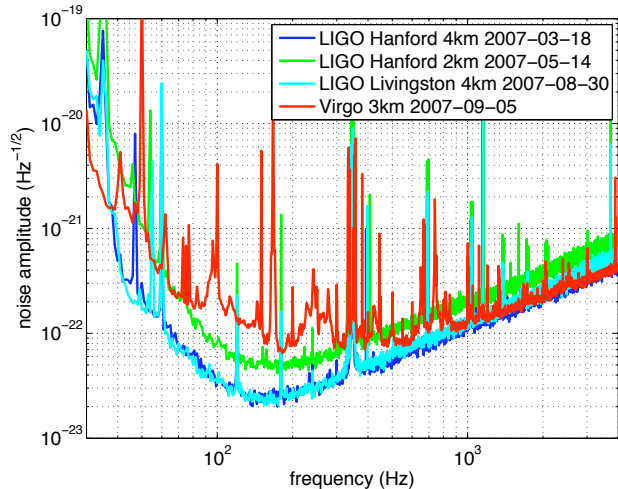


FIG. 1.— Representative noise spectra from the LIGO and Virgo detectors during S5-VSR1.

strain, with two polarization components. Data from each interferometer record the length difference of the arms and, when calibrated, measure the strain induced by a gravitational wave. These data are in the form of a time series, digitized at a sample rate of 16384 s^{-1} (LIGO) or 20000 s^{-1} (Virgo). The response of an interferometer to a given strain is measured by injecting sinusoidal excitations with known amplitude into the test mass control systems and tracking the resulting signals at the measurement point throughout each run. The result is a measurement of the time-varying, frequency-dependent response function of each interferometer.

The fifth LIGO science run (S5) was held from 2005 November 4 to 2007 October 1. During this run, over one year of science-quality data was collected with all three LIGO interferometers in simultaneous operation. The LIGO interferometers operated at their design sensitivity, with duty factors of 75%, 76%, and 65% for the H1, H2, and L1 interferometers. The Virgo detector started its first science run (VSR1) on 2007 May 18. The Virgo duty cycle over VSR1 was 78%. Figure 1 shows representative sensitivities, in terms of noise spectral density, of the LIGO and Virgo interferometers during the run. All of the instruments ran together continuously until 2007 October 1, amounting to about 4.5 months of joint data taking.

The GEO 600 detector (Grote et al. 2008), located near Hannover, Germany, was also operational during the S5-VSR1 run, though with a lower sensitivity than LIGO and Virgo. We do not use the GEO data in this search as the modest gains in the sensitivity to gravitational wave signals would not have offset the increased complexity of the analysis.

3. GRB SAMPLE

The GRB triggers that were contemporaneous with the S5-VSR1 run came mostly from the *Swift* satellite (Gehrels et al. 2004), but several triggers also came from other IPN satellites (Hurley et al. 2009), including HETE-2 (Ricker et al. 2003), and INTEGRAL (Winkler et al. 2003). We obtained our GRB triggers through the Gamma-ray Burst Coordinates Network (GCN 2007). During the S5-VSR1 run, there were a total of 212 GRBs reported by these satellite-based gamma-ray ex-

periments. Of these, 33 were short-duration GRBs, and 59 had associated redshift measurements. All but 4 of these GRBs had well-defined positions.

Only LIGO and Virgo data which are of science-mode quality are analyzed. These are data collected when the interferometers are in a stable, resonant configuration. Additionally, data segments which are flagged as being of poor quality are not included in the analysis. A full analysis (detection search and upper limit calculation) is performed for all GRBs which have well-defined positions and for which at least two interferometers have science-mode data passing quality requirements. There are 137 such GRBs, of which 21 are short-duration bursts, and 35 have measured redshifts. A list of the GRBs and relevant information are given in Table 1 in Appendix A.

4. SEARCH PROCEDURE

4.1. Overview

The basic search procedure follows that used in recent LIGO GRB searches (Abbott et al. 2008b,a). All GRBs are treated identically, without regard to their duration, or redshift (if known), or fluence. We use the interval from 120 s before each GRB trigger time to 60 s after as the window in which to search for an associated gravitational-wave burst. This conservative window is large enough to take into account most reasonable time delays between a gravitational-wave signal from a progenitor and the onset of the gamma-ray signal. It is also safely larger than any uncertainty in the definition of the measured GRB trigger time. The data in this search window are called the *on-source* data.

The on-source data are scanned by an algorithm designed to detect transients that may have been caused by a gravitational-wave burst. In this search, two algorithms are used: the cross-correlation algorithm used in previous LIGO searches (Abbott et al. 2008b), and X-PIPELINE¹, a new coherent analysis package (Chatterji et al. 2006; Sutton et al. 2009). The cross-correlation algorithm correlates the data between pairs of detectors, while X-PIPELINE combines data from arbitrary sets of detectors, taking into account the antenna response and noise level of each detector to improve the search sensitivity.

The data are analysed independently by X-PIPELINE and the cross-correlation algorithm to produce lists of transients, or *events*, that may be candidate gravitational-wave signals. Each event is characterised by a measure of significance, based on energy (X-PIPELINE) or correlation between detectors (cross-correlation algorithm). To reduce the effect of non-stationary background noise, the list of candidate events is subjected to checks that “veto” events overlapping in time with known instrumental or environmental disturbances (Abbott et al. 2009b). X-PIPELINE also applies additional consistency tests based on the correlations between the detectors to further reduce the number of background events. The surviving event with the largest significance is taken to be the best candidate for a gravitational-wave signal for that GRB; it is referred to as the *loudest event* (Brady et al. 2004; Biswas et al. 2009).

¹ <https://geco.phys.columbia.edu/xpipeline/browser?rev=2634>

To estimate the expected distribution of the loudest events under the null hypothesis, the pipelines are also applied to all coincident data within a 3 h period surrounding the on-source data. This data for background estimation is called the *off-source* data. Its proximity to the on-source data makes it likely that the estimated background will properly reflect the noise properties in the on-source segment. The off-source data are processed identically to the on-source data; in particular, the same data-quality cuts and consistency tests are applied, and the same sky position relative to the Earth is used. To increase the off-source distribution statistics, multiple time shifts are applied to the data streams from different detector sites (or between the H1 and H2 streams for GRBs occurring when only those two detectors were operating), and the off-source data are re-analysed for each time shift. For each 180 s segment of off-source data, the loudest surviving event is determined. The distribution of significances of the loudest background events, $C(\mathcal{S}_{\max})$, thus gives us an empirical measure of the expected distribution of the significance of the loudest on-source event $\mathcal{S}_{\max}^{\text{on}}$ under the null hypothesis.

To determine if a GWB is present in the on-source data, the loudest on-source event is compared to the background distribution. If the on-source significance is larger than that of the loudest event in 95% of the off-source segments (i.e., if $C(\mathcal{S}_{\max}^{\text{on}}) \geq 0.95$), then the event is considered as a candidate gravitational-wave signal. Candidate signals are subjected to additional “detection checklist” studies to try to determine the physical origin of the event; these studies may lead to rejecting the event as being of terrestrial origin, or they may increase our degree of confidence in it being due to a gravitational wave.

Regardless of whether a statistically significant signal is present, we also set a frequentist upper limit on the strength of gravitational waves associated with the GRB. For a given gravitational-wave signal model, we define the 90% confidence level upper limit on the signal amplitude as the minimum amplitude for which there is a 90% or greater chance that such a signal, if present in the on-source region, would have produced an event with significance larger than the largest value $\mathcal{S}_{\max}^{\text{on}}$ actually measured. The signal models simulated are discussed in Sec. 6.1.

Since X-PIPELINE was found to be more sensitive to GWBs than the cross-correlation pipeline (by about a factor of 2 in amplitude), we decided in advance to set the upper limits using the X-PIPELINE results. The cross-correlation pipeline is used as a detection-only search. Since it was used previously for the analysis of a large number of GRBs during S2-S4, and for GRB070201 during S5, including the cross-correlation pipeline provides continuity with past GRB searches and allows comparison of X-PIPELINE with the technique used for these past searches.

4.2. X-PIPELINE

X-PIPELINE is a MATLAB-based software package for performing coherent searches for gravitational-wave bursts in data from arbitrary networks of detectors. Since X-PIPELINE has not previously been used in a published LIGO or Virgo search, in this section we give a brief overview of the main steps followed in a GRB-

triggered search. For more details on X-PIPELINE, see Sutton et al. (2009).

Coherent techniques for GWB detection (see for example Gursel & Tinto 1989; Flanagan & Hughes 1998; Anderson et al. 2001; Klimentko et al. 2005, 2006; Mohanty et al. 2006; Rakhmanov 2006; Chatterji et al. 2006; Summerscales et al. 2008) combine data from multiple detectors before scanning it for candidate events. They naturally take into account differences in noise spectrum and antenna response of the detectors in the network. X-PIPELINE constructs several different linear combinations of the data streams: those that maximize the expected signal-to-noise ratio for a GWB of either polarization from a given sky position (referred to as the d_+ and d_\times streams), and those in which the GWB signal cancels (referred to as the d_{null} streams). It then looks for transients in the d_+ and d_\times streams. Later, the energies in the d_+ , d_\times , and d_{null} streams are compared to attempt to discriminate between true GWBs and background noise fluctuations.

4.2.1. Event Generation

X-PIPELINE processes data in 256 s blocks. First, it whitens the data from each detector using linear predictor error filters (Chatterji et al. 2004). It then time-shifts each stream according to the time-of-flight for a gravitational wave incident from the sky position of the GRB, so that a gravitational-wave signal will be simultaneous in all the data streams after the shifting. The data are divided into 50% overlapping segments and Fourier transformed. X-PIPELINE then coherently sums and squares these Fourier series to produce time-frequency maps of the energy in the d_+ , d_\times , and d_{null} combinations. Specifically, we define the noise-weighted antenna response vectors $\mathbf{f}^{+, \text{DPF}}$ and $\mathbf{f}^{\times, \text{DPF}}$ for the network, with components

$$f_\alpha^{+, \text{DPF}}(\theta, \phi, f) = \frac{F_\alpha^+(\theta, \phi, \psi^{\text{DPF}})}{\sqrt{S_\alpha(f)}}, \quad (1)$$

$$f_\alpha^{\times, \text{DPF}}(\theta, \phi, f) = \frac{F_\alpha^\times(\theta, \phi, \psi^{\text{DPF}})}{\sqrt{S_\alpha(f)}}. \quad (2)$$

Here (θ, ϕ) is the direction to the GRB, ψ^{DPF} is the polarization angle specifying the orientation of the plus and cross polarizations, F_α^+ , $F_\alpha^\times \in [-1, 1]$ are the antenna response factors to the plus and cross polarizations (Anderson et al. 2001, see also Sec. 6.1), and S_α is the noise power spectrum of detector α . DPF stands for the dominant polarization frame; this is a frequency-dependent polarization basis $\psi^{\text{DPF}}(f)$ such that $\mathbf{f}^{+, \text{DPF}} \cdot \mathbf{f}^{\times, \text{DPF}} = 0$ and $|\mathbf{f}^{+, \text{DPF}}| \geq |\mathbf{f}^{\times, \text{DPF}}|$ (Klimentko et al. 2005). With this choice of basis, the d_+ stream is defined as the projection

$$d_+ \equiv \frac{\mathbf{f}^{+, \text{DPF}} \cdot \mathbf{d}}{|\mathbf{f}^{+, \text{DPF}}|}, \quad (3)$$

where \mathbf{d} is the set of whitened data streams from the individual detectors. The “signal energy” $E_+ \equiv |d_+|^2$ can be shown to be the sum-squared signal-to-noise ratio in the network corresponding to the least-squares estimate of the h_+ polarization of the gravitational wave in the

dominant polarization frame. The d_{\times} stream and energy E_{\times} are defined analogously. The sum $E_{+} + E_{\times}$ is then the maximum sum-squared signal-to-noise at that frequency that is consistent with a GWB arriving from the given sky position at that time.

The projections of the data orthogonal to $\mathbf{f}^{+, \text{DPF}}$, $\mathbf{f}^{\times, \text{DPF}}$ yield the null streams, in which the contributions of a real gravitational wave incident from the given sky position will cancel. The null stream energy $E_{\text{null}} \equiv |d_{\text{null}}|^2$ should therefore be consistent with background noise. (The definition of the null streams is independent of the polarization basis used.) The number of independent data combinations yielding null streams depends on the geometry of the network. Networks containing both the H1 and H2 interferometers have one null stream combination. Networks containing L1, V1, and at least one of H1 or H2 have a second null stream. For the H1-H2-L1-V1 network there are two independent null streams; in this case we sum the null energy maps from the two streams to yield a single null energy.

Events are selected by applying a threshold to the $E_{+} + E_{\times}$ map, so that the pixels with the 1% highest values are marked as *black pixels*. Nearest-neighbor black pixels are grouped together into clusters (Sylvestre 2002). These clusters are our events. Each event is assigned an approximate statistical significance \mathcal{S} based on a χ^2 distribution; for Gaussian noise in the absence of a signal, $2(E_{+} + E_{\times})$ is χ^2 -distributed with $4N_{\text{pix}}$ degrees of freedom, where N_{pix} is the number of pixels in the event cluster. This significance is used when comparing different clusters to determine which is the “loudest”. The various coherent energies (E_{+} , E_{\times} , E_{null}) are summed over the component pixels of the cluster, and other properties such as duration and bandwidth of the cluster are also recorded.

The analysis of time shifting, FFTing, and cluster identification is repeated for FFT lengths of (1/8, 1/16, 1/32, 1/64, 1/128, 1/256) s, to cover a range of possible GWB durations. Clusters produced by different FFT lengths that overlap in time and frequency are compared. The cluster with the largest significance is kept; the others are discarded. Finally, only clusters with central time in the on-source window of 120 s before the GRB time to 60 s after are considered as possible candidate events.

4.2.2. Glitch Rejection

Real detector noise contains *glitches*, which are short transients of excess strain noise that can masquerade as GWB signals. As shown in Chatterji et al. (2006), one can construct tests that are effective at rejecting glitches. Specifically, each coherent energy E_{+} , E_{\times} , E_{null} has a corresponding “incoherent” energy I_{+} , I_{\times} , I_{null} that is formed by discarding the cross-correlation terms ($d_{\alpha} d_{\beta}^*$) when computing $E_{+} = |d_{+}|^2$, etc. For large-amplitude background noise glitches the coherent and incoherent energies are strongly correlated, $E \sim I \pm \sqrt{I}$. For strong gravitational-wave signals one expects either $E_{+} > I_{+}$ and $E_{\times} < I_{\times}$ or $E_{+} < I_{+}$ and $E_{\times} > I_{\times}$ depending on the signal polarization content, and $E_{\text{null}} < I_{\text{null}}$.

X-PIPELINE uses the incoherent energies to apply a pass/fail test to each event. A nonlinear curve is fit to the measured distribution of background events used for tun-

ing (discussed below); specifically, to the median value of I as a function of E . Each event is assigned a measure of how far it is above or below the median:

$$\sigma \equiv (I - I_{\text{med}}(E))/I^{1/2}. \quad (4)$$

For $(I_{\text{null}}, E_{\text{null}})$, an event is passed if $\sigma_{\text{null}} > r_{\text{null}}$, where r_{null} is some threshold. For (I_{+}, E_{+}) and (I_{\times}, E_{\times}) , the event passes if $|\sigma_{+}| > r_{+}$ and $|\sigma_{\times}| > r_{\times}$. (For the H1-H2 network, which contains only aligned interferometers, the conditions are $\sigma_{+} < r_{+}$ and $\sigma_{\text{null}} > r_{\text{null}}$.) An event may be tested for one, two, or all three of the pairs $(I_{\text{null}}, E_{\text{null}})$, (I_{+}, E_{+}) , and (I_{\times}, E_{\times}) , depending on the GRB. The choice of which energy pairs are tested and the thresholds applied are determined independently for each of the 137 GRBs. X-PIPELINE makes the selection automatically by comparing simulated GWBs to background noise events, as discussed below. In addition, the criterion $I_{\text{null}} \geq 1.2E_{\text{null}}$ was imposed for all H1-H2 GRBs, as this was found to be effective at removing loud background glitches without affecting simulated gravitational waves.

In addition to the coherent glitch vetoes, events may also be rejected because they overlap *data quality flags* or *veto*s, as mentioned in Sec. 4.1. The flags and vetoes used are discussed in Abbott et al. (2009b). To avoid excessive dead time due to poor data quality, we impose minimum criteria for a detector to be included in the network for a given GRB. Specifically, at least 95% of the 180 s of on-source data must be free of data quality flags and vetoes, and all of the 6 s spanning the interval from -5 to +1 s around the GRB trigger must be free of flags and vetoes.

4.2.3. Pipeline Tuning

To detect a gravitational wave, X-PIPELINE compares the largest significance of all events in the on-source time after application of vetoes, $\mathcal{S}_{\text{max}}^{\text{on}}$, to the cumulative distribution $C(\mathcal{S}_{\text{max}})$ of loudest significances measured in each off-source segment. If $C(\mathcal{S}_{\text{max}}^{\text{on}}) \geq 0.95$, we consider the event for follow-up study.

To maximize the sensitivity of X-PIPELINE, we tune the coherent glitch test thresholds r_{+} , r_{\times} , r_{null} for each GRB to optimize the trade-off between glitch rejection and signal acceptance. We do this using the off-source data and data containing simulated GWB signals (*injections*, discussed in Sec. 6.1), but not the on-source data. This *blind* tuning avoids the possibility of biasing the upper limit.

The procedure is simple. The off-source segments and injections are divided randomly into two equal sets: half for tuning, and half for sensitivity and background estimation. Each of r_{+} , r_{\times} , and r_{null} are tested with trial thresholds of $[0, 0.5, 1, 1.5, \dots, 5]$, where a value of 0 is treated as not testing that energy type. For each of the $11^3 = 1331$ possible combinations of trial thresholds, the loudest surviving event in each tuning off-source segment is found. The injection amplitude required for 90% of the injections to be louder than the 95th percentile of \mathcal{S}_{max} is computed for each waveform type. The set of thresholds giving the lowest required injection amplitude over all waveforms is selected as optimal (at least one of r_{+} , r_{\times} , and r_{null} is required to be non-zero). To get an unbiased estimate of the expected sensitivity and background, we apply the tuned vetoes to the second set of off-source

segments and injections, that were not used for tuning. For more details, see Sutton et al. (2009).

4.3. Cross-Correlation Pipeline

The cross-correlation pipeline has been used in two previous LIGO searches (Abbott et al. 2008b,a) for GWBs associated with GRBs, and is described in detail in these references. We therefore give only a brief summary of the pipeline here.

In the present search, the cross-correlation pipeline is applied to the LIGO detectors only. (The different orientation and noise spectrum shape of Virgo relative to the LIGO detectors is more easily accounted for in a coherent analysis.) The 180 s on-source time series for each interferometer is whitened as described in Abbott et al. (2008b) and divided into time bins, then the cross-correlation for each interferometer pair and time bin is calculated. The cross-correlation cc of two timeseries s_1 and s_2 is defined as

$$cc = \frac{\sum_{i=1}^m [s_1(i) - \mu_1][s_2(i) - \mu_2]}{\sqrt{\sum_{j=1}^m [s_1(j) - \mu_1]^2} \sqrt{\sum_{k=1}^m [s_2(k) - \mu_2]^2}}, \quad (5)$$

where μ_1 and μ_2 are the corresponding means, and m is the number of samples in the bin. Cross-correlation bins of lengths 25 ms and 100 ms are used to target short-duration GW signals with durations of ~ 1 ms to ~ 100 ms. The bins are overlapped by half a bin width to avoid loss of signals occurring near a bin boundary. Each LHO-LLO pair of 180 s on-source segments is shifted in time relative to each other to account for the time-of-flight between the detector sites for the known sky position of the GRB before the cross-correlations are calculated.

The cross-correlation is calculated for each interferometer pair and time bin for each bin length used. For an H1-H2 search the largest cross-correlation value obtained within the 180 s search window is considered the most significant measurement. For an H1-L1 or H2-L1 search, the largest *absolute* value of the cross-correlation is taken as the most significant measurement. This was done to take into account the possibility that signals at LHO and LLO could be anticorrelated depending on the (unknown) polarization of the gravitational wave.

5. SEARCH RESULTS

5.1. Per-GRB Results

The results of the search for each of the 137 GRBs analysed by X-PIPELINE are shown in Table 1, Appendix A. The seventh column in this table lists the *local probability* $p \equiv 1 - C(\mathcal{S}_{\max}^{\text{on}})$ for the loudest on-source event, defined as the fraction of background trials that produced a more significant event (a “—” indicates no event survived all cuts). Five GRBs had events passing the threshold of $p = 0.05$ to become candidate signals.

Since the local probability is typically estimated using approximately 150 off-source segments, small p values are subject to relatively large uncertainty from Poisson statistics. We therefore applied additional time-shifts to the off-source data to obtain a total of 18000 off-source segments for each candidate which were processed to improve the estimate of p . The 5 GRBs and their refined local probabilities are 060116 ($p = 0.0402$), 060510B (0.0124), 060807 (0.00967), 061201 (0.0222), and 070529

(0.0776). (Note that for GRB 070529, the refined local probability from the extra off-source segments was *larger* than the threshold of 0.05 for candidate signals.)

Considering that we analysed 137 GRBs, these numbers are consistent with the null hypothesis that no gravitational-wave burst signal is associated with any of the GRBs tested. In addition, three of these GRBs have large measured redshift: GRB 060116 ($z = 6.6$), 060510B ($z = 4.9$), and 070529 ($z = 2.5$), making it highly unlikely *a priori* that we would expect to see a GWB in these cases. Nevertheless, each event has been subjected to follow-up examinations. These include checks of the consistency of the candidate with background events (such as in coherent energies, and frequency), checks of detector performance at the time as indicated by monitoring programs and operator logs, and scans of data from detector and environmental monitoring equipment to look for anomalous behavior. In each case, the candidate event appears consistent with the coherent energy distributions of background events, lying just outside the coherent glitch rejection thresholds. The frequency of each event is also typical of background events for their respective GRBs. Some of these GRBs occurred during periods of elevated background noise, and one occurred during a period of glitchy data in H1. In two cases scans of data from monitoring equipment indicate a possible physical cause for the candidate event: one from non-stationarity in a calibration line, and another due to up-conversion of low-frequency noise in H1.

All but two of the GRBs processed by X-PIPELINE are also analysed by the cross-correlation pipeline. The cross-correlation pipeline produces a local probability for each detector pair and for each bin length (25 ms and 100 ms), for a total of 646 measurements from 135 GRBs. The threshold on the cross-correlation local probability corresponding to the 5% threshold for X-PIPELINE is therefore $5\% \times 135/646 \simeq 1\%$. A total of 7 GRBs have $p < 1\%$ from cross-correlation: 060306 (0.00833), 060719 (0.00669), 060919 (0.00303), 061110 (0.00357), 070704 (0.00123), and 070810 (0.00119). These results are also consistent with the null hypothesis. Furthermore, none of these GRBs are among those that had a low p value from X-PIPELINE. This is further indication that the candidate events detected by each pipeline are due to background noise rather than GWBs. Specifically, X-PIPELINE and the cross-correlation pipeline use different measures of significance of candidate events. Whereas a strong GWB should be detected by both, any given background noise fluctuation may have very different significance in the two pipelines.

We conclude that we have not identified a plausible gravitational-wave burst signal associated with any of the 137 GRBs tested.

5.2. Binomial Test

Gravitational-wave signals from individual GRBs are likely to be very weak in most cases due to the cosmological distances involved. Therefore, besides searching for GWB signals from each GRB, we also test for a cumulative signature associated with a sample of several GRBs (Finn et al. 1999). This approach has been used in Astone et al. (2002, 2005) to analyze resonant mass detector data using triggers from the BATSE and BeppoSAX missions, and more recently in the LIGO search

for GRBs during the S2, S3, and S4 science runs (Abbott et al. 2008b).

Under the null hypothesis (no GWB signal), the local probability for each GRB is expected to be uniformly distributed on $[0, 1]$. Moderately strong GWBs associated with one or more of the GRBs will cause the low- p tail of the distribution to deviate from that expected under the null hypothesis. We apply the binomial test used in Abbott et al. (2008b) to search for a statistically significant deviation, applying it to the $5\% \times 137 \simeq 7$ least probable (lowest p) on-source results in the GRB distribution. Briefly, we sort the 7 smallest local probabilities in increasing order, p_1, p_2, \dots, p_7 . For each p_i we compute the binomial probability $P_{\geq i}(p_i)$ of getting i or more events out of 137 at least as significant as p_i . The smallest $P_{\geq i}(p_i)$ is selected as the most significant deviation from the null hypothesis. To account for the trials factor from testing 7 values of i , we repeat the test many times using 137 fake local probabilities drawn from uniform discrete distributions corresponding to the number of off-source segments for each GRB (18000 for our refined p estimates). The probability associated with the actual smallest $P_{\geq i}(p_i)$ is defined as the fraction of Monte Carlo trials that gave binomial probabilities as small or smaller. Note that this procedure also automatically handles the case of a single loud GWB.

In addition to the 5 “candidate” GRBs, extra time-shifted off-source segments were analysed for the 2 GRBs with the next smallest local probabilities, GRB 060428B (0.0139) and 060930 ($p = 0.0248$). (By chance, for both of these GRBs the refined local probabilities from the extra off-source segments are *smaller* than the threshold of 0.05 for candidate signals, though the original estimates were larger.) Together with the 5 candidates, this gives the 7 refined local probabilities 0.00967, 0.0124, 0.0139, 0.0222, 0.0248, 0.0402, 0.0776. The associated smallest binomial probability is $P_{\geq 5}(0.0248) = 0.259$. Approximately 56% of Monte Carlo trials give binomial probabilities this small or smaller, hence we conclude that there is no significant deviation of the measured local probabilities from the null hypothesis. For comparison, Figure 2 shows the distribution of local probabilities for all GRBs, as well as the values that would need to be observed to give only 1% consistency with the null hypothesis.

Similar results are found when restricting the test to GRBs without measured redshift. In this case the smallest binomial probability is $P_{\geq 4}(0.0248) = 0.252$ with 48% of Monte Carlo trials yielding binomial probabilities this small or smaller. Analysis of the cross-correlation local probabilities also shows no significant deviation. Combining the local probabilities from the 25 ms and 100 ms analyses, we find the smallest binomial probability to be $P_{\geq 2}(0.00123) = 0.190$ with 52% of Monte Carlo trials yielding binomial probabilities this small or smaller.

6. UPPER LIMITS

The sensitivity of the search to gravitational waves is determined by a Monte Carlo analysis. For each GRB, we add (or “inject”) simulated GWB signals into the detector data and repeat the analysis. We count an injected signal as “detected” if it produces an event that is louder than the loudest on-source event within 100 ms of the injection time. (When tuning, we do not know the significance of the loudest on-source event. We therefore

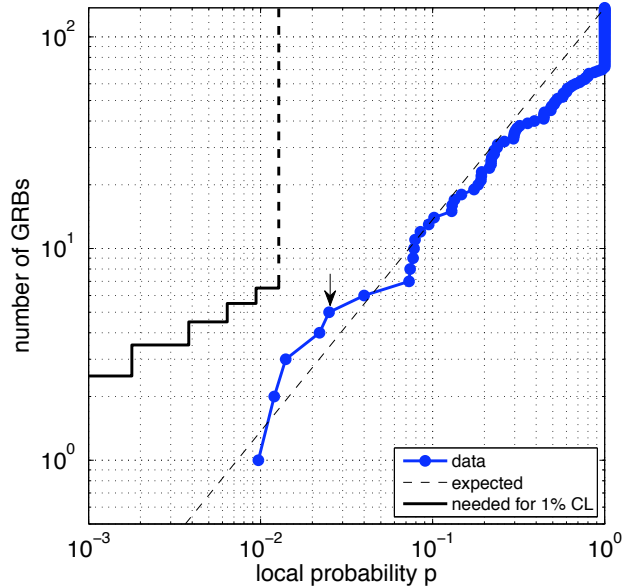


FIG. 2.— Cumulative local probability distribution resulting from the search of 137 GRBs with X-PIPELINE. The most significant excess is indicated by the arrow. The expected distribution under the null hypothesis is indicated by the diagonal dashed line. The excess needed for a 1% confidence in the null hypothesis is indicated by the solid line. The maximum excess indicated by this line is 7 events because only the 7 most significant events in the actual distribution are tested. The buildup of GRBs at $p = 1$ occurs because approximately half of the GRBs do not have any event surviving all the analysis cuts.

count an injection as detected if it is louder than the median background loudest event from the off-source tuning segments; *i.e.*, louder than the 50th percentile of the sample of \mathcal{S}_{\max} values.) For a given waveform morphology, we define the 90% confidence level upper limit on the signal amplitude as the minimum amplitude for which the detection probability is 0.9 or greater.

We discuss the signal models in Sec. 6.1, their systematic uncertainties in Sec. 6.2, and the upper limit results in Sec. 6.3.

6.1. Simulations

The antenna response of an interferometer to a gravitational wave with polarization strains $h_+(t)$ and $h_\times(t)$ depends on the polarization basis angle ψ and the direction (θ, ϕ) to the source as

$$h(t) = F_+(\theta, \phi, \psi)h_+(t) + F_\times(\theta, \phi, \psi)h_\times(t). \quad (6)$$

Here $F_+(\theta, \phi, \psi)$, $F_\times(\theta, \phi, \psi)$ are the plus and cross antenna factors introduced in Sec. 4.2; see Anderson et al. (2001) for explicit definitions.

A convenient measure of the gravitational-wave amplitude is the root-sum-square amplitude,

$$h_{\text{rss}} = \sqrt{\int (|h_+(t)|^2 + |h_\times(t)|^2) dt}. \quad (7)$$

The energy flux (power per unit area) of the wave is (Isaacson 1968)

$$F_{\text{GW}} = \frac{c^3}{16\pi G} \langle (\dot{h}_+)^2 + (\dot{h}_\times)^2 \rangle, \quad (8)$$

where the angle brackets denote an average over several periods. The total energy emitted assuming isotropic

emission is then

$$E_{\text{GW}}^{\text{iso}} = 4\pi D^2 \int dt F_{\text{GW}}, \quad (9)$$

where D is the distance to the source.

The forms of $h_+(t)$ and $h_\times(t)$ depend on the type of simulated waveform. It is likely that many short GRBs are produced by the merger of neutron-star–neutron-star or black-hole–neutron-star binaries; the gravitational-wave signal from inspiralling binaries is fairly well understood (Blanchet 2006; Aylott et al. 2009), and progress is being made on modelling the merger phase (Etienne et al. 2008; Baiotti et al. 2008). For other progenitor types, particularly for long GRBs, there are no robust models for the gravitational-wave emission (see for example Fryer et al. 2002; Kobayashi & Meszaros 2003; van Putten et al. 2004; Ott 2009, for possible scenarios). Since our detection algorithm is designed to be sensitive to generic gravitational-wave bursts, we choose simple *ad hoc* waveforms for tuning and testing. Specifically, we use sine-Gaussian and cosine-Gaussian waveforms:

$$h_+(t + t_0) = h_{+,0} \sin(2\pi f_0 t) \exp\left(\frac{-(2\pi f_0 t)^2}{2Q^2}\right), \quad (10)$$

$$h_\times(t + t_0) = h_{\times,0} \cos(2\pi f_0 t) \exp\left(\frac{-(2\pi f_0 t)^2}{2Q^2}\right), \quad (11)$$

where t_0 is the central time, f_0 is the central frequency, $h_{+,0}$ and $h_{\times,0}$ are the amplitude parameters of the two polarizations, and Q is a dimensionless constant which represents roughly the number of cycles with which the waveform oscillates with more than half of the peak amplitude. For $Q \gtrsim 3$, the root-sum-squared amplitude of this waveform is

$$h_{\text{rss}} \approx \sqrt{\frac{Q(h_{+,0}^2 + h_{\times,0}^2)}{4\pi^{1/2} f_0}} \quad (12)$$

and the energy in gravitational waves is

$$E_{\text{GW}}^{\text{iso}} \approx \frac{\pi^2 c^3}{G} D^2 f_0^2 h_{\text{rss}}^2. \quad (13)$$

Using these waveforms for $h_+(t)$ and $h_\times(t)$, we simulate circularly polarized GW waves by setting the sine-Gaussian and cosine-Gaussian amplitudes equal to each other, $h_{+,0} = h_{\times,0}$. To simulate linearly polarized waves, we set $h_{\times,0} = 0$.

The peak time of the simulated signals is distributed uniformly through the on-source interval. We use $Q = 2^{3/2}\pi = 8.9$, a standard choice in LIGO burst searches. The polarization angle ψ for which h_+ , h_\times take the forms in equations (10) and (11) is uniform on $[0, \pi)$, and the sky position used is that of the GRB (fixed in right ascension and declination). We simulate signals at discrete log-spaced amplitudes, with 500 injections of each waveform for each amplitude.

Early tests of the search algorithms used the central frequencies $f_0 = (100, 150, 250, 554, 1000, 1850)$ Hz, and both linearly and circularly polarized injections. The final X-PIPELINE tuning (performed after implementation of an improved data-whitening procedure) uses 150 Hz and 1000 Hz injections of both polarizations.

6.2. Statistical and Systematic Errors

Our upper limit on gravitational-wave emission by a GRB is $h_{\text{rss}}^{90\%}$, the amplitude at which there is a 90% or greater chance that such a signal, if present in the on-source region, would have produced an event with significance larger than the largest actually measured. There are several sources of error, both statistical and systematic, that can affect our limits. These are calibration uncertainties (amplitude and phase response of the detectors, and relative timing errors), uncertainty in the sky position of the GRB, and uncertainty in the measurement of $h_{\text{rss}}^{90\%}$ due to the finite number of injections and the use of a discrete set of amplitudes.

To estimate the effect of these errors on our upper limits, we repeat the Monte Carlo runs for a subset of the GRBs, simulating all three of these types of errors. Specifically, the amplitude, phase, and time delays for each injection in each detector are perturbed by Gaussian-distributed corrections matching the calibration uncertainties for each detector. The sky position is perturbed in a random direction by a Gaussian-distributed angle with standard deviation of 3 arcmin. Finally, the discrete amplitudes used are offset by those in the standard analysis by a half-step in amplitude. The perturbed injections are then processed, and the open-box upper limit produced using the same coherent consistency test tuning as in the actual open-box search. The typical difference between the upper limits for perturbed injections and unperturbed injections then gives an estimate of the impact of the errors on our upper limits.

For low-frequency injections (at 150 Hz) we find that the ratio of the upper limit for perturbed injections to unperturbed injections is 1.03 with a standard deviation of 0.06. We therefore increase the estimated upper limits at 100 Hz by a factor of $1.03 + 1.28 \times 0.06 = 1.10$ as a conservative allowance for statistical and systematic errors (the factor 1.28 comes from the 90% upper limit for a Gaussian distribution). The dominant contribution is due to the finite number of injections. For the high-frequency (1000 Hz) injections the factor is $1.10 + 1.28 \times 0.12 = 1.25$. In addition to finite-number statistics, the calibration uncertainties are more important at high frequencies and make a significant contribution to this factor. All limits reported in this paper include these allowance factors.

6.3. Limits on Strain and Distance

The upper limits on GWB amplitude and lower limits on the distance for each of the GRBs analysed are given in Table 1 in Appendix A. These limits are computed for circularly polarized 150 Hz and 1000 Hz sine-Gaussian waveforms. We compute the distance limits by assuming the source emitted $E_{\text{GW}}^{\text{iso}} = 0.01 M_\odot c^2 = 1.8 \times 10^{52}$ erg of energy isotropically in gravitational waves and use equation (13) to infer a lower limit on D . We choose $E_{\text{GW}}^{\text{iso}} = 0.01 M_\odot c^2$ because this is a reasonable value one might expect to be emitted in the LIGO-Virgo band by various progenitor models. For example, mergers of neutron-star binaries or neutron-star–black-hole binaries (the likely progenitors of most short GRBs) will have isotropic-equivalent emission of order $(0.01 - 0.1) M_\odot c^2$ in the 100-200 Hz band. For long GRBs, fragmentation of the accretion disk (Davies et al. 2002; King et al. 2005; Piro & Pfahl 2007) could produce inspiral-like chirps

with $(0.001 - 0.01) M_{\odot}c^2$ emission. The suspended accretion model (van Putten et al. 2004) also predicts an energy emission of up to $(0.01 - 0.1)M_{\odot}c^2$ in this band. For other values of $E_{\text{GW}}^{\text{iso}}$ the distance limit scales as $D \propto (E_{\text{GW}}^{\text{iso}})^{1/2}$.

As can be seen from Table 1, the strongest limits are on gravitational-wave emission at 150 Hz, where the sensitivity of the detectors is best (see Figure 1). Figure 3 shows a histogram of the distance limits for the 137 GRBs tested. The typical limits at 150 Hz from the X-PIPELINE analysis are (10–20) Mpc. The best upper limits are for GRBs later in S5-VSR1, when the detector noise levels tended to be lowest (and when the most detectors were operating), and for GRBs that occurred at sky positions for which the detector antenna responses F_+ , F_{\times} were best. The strongest limits obtained were for GRB 070429B: $h_{\text{rss}}^{90\%} = 1.75 \times 10^{-22} \text{Hz}^{-1/2}$, $D^{90\%} = 26.2$ Mpc at 150 Hz. For comparison, the smallest measured redshift in our GRB sample is for 060614, which had $z = 0.125$ (Price et al. 2006) or $D \simeq 578$ Mpc (Wright 2006). (Though GRB 060218 at $z = 0.0331$ (Mirabal et al. 2006) occurred during S5, unfortunately, the LIGO-Hanford and Virgo detectors were not operating at the time.)

A GRB of particular interest is 070201. This short-duration GRB had a position error box overlapping M31 (see Mazets et al. 2008, and references therein), which is at a distance of only 770 kpc. An analysis of LIGO data from this time was presented in Abbott et al. (2008a). GRB 070201 was included in the present search using the new X-PIPELINE search package. Our new upper limits on the amplitude of a GWB associated with GRB 070201 are $h_{\text{rss}}^{90\%} = 6.38 \times 10^{-22} \text{Hz}^{-1/2}$ at 150 Hz, and $h_{\text{rss}}^{90\%} = 27.8 \times 10^{-22} \text{Hz}^{-1/2}$ at 1000 Hz. These are approximately a factor of 2 lower than those placed by the cross-correlation algorithm. For a source at 770 kpc, the energy limit from equation (13) is $E_{\text{GW}}^{\text{iso}} = 1.15 \times 10^{-4} M_{\odot}c^2$ at 150 Hz. While about a factor of 4 lower than the GWB limit presented in Abbott et al. (2008a), this is still several orders of magnitude away from being able to test the hypothesis that this GRB’s progenitor was a soft-gamma repeater in M31 (Mazets et al. 2008).

7. SUMMARY AND CONCLUSION

We have presented the results of a search for gravitational-wave bursts associated with 137 GRBs that occurred during the LIGO Science Run 5 – Virgo Science Run 1, from 2005 November 4 to 2007 October 1. The search used two independent data-analysis pipelines to scan for unmodelled transient signals consistent with the known time and sky position of each GRB. No plausible gravitational-wave signals were identified. Assuming isotropic gravitational-wave emission by the progenitor, we place lower limits on the distance to each GRB. Typical limits are $D \sim 15$ Mpc $(E_{\text{GW}}^{\text{iso}}/0.01 M_{\odot}c^2)^{1/2}$ for emission at frequencies around 150 Hz, where the LIGO-Virgo detector network has best sensitivity.

It is informative to compare this result to the rate density of GRBs (see, for example, Leonor et al. 2009). For long GRBs, a commonly used estimate of the local rate density (the rate of observable GRBs per unit volume)

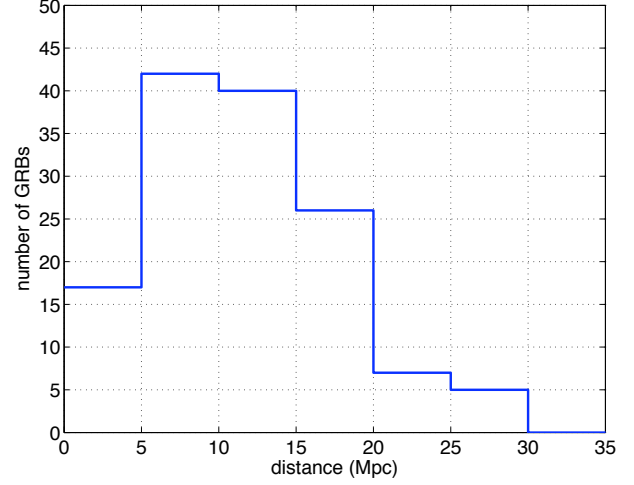


FIG. 3.— Histogram of lower limits on the distance to each of the 137 GRBs studied, assuming that the GRB progenitors emit $0.01 M_{\odot}c^2 = 1.8 \times 10^{52} \text{erg}$ of energy in circularly polarized gravitational waves at 150 Hz.

is $R_{\text{long}}^{\text{obs}} \sim 0.5 \text{ Gpc}^{-3} \text{yr}^{-1}$ (Sokolov 2001; Schmidt 2001; Le & Dermer 2007). We therefore estimate the *a priori* expected number of long GRBs being observed within a distance D during a two-year science run as

$$\langle N_{\text{long}} \rangle \simeq R_{\text{long}}^{\text{obs}} \left(\frac{4}{3} \pi D^3 \right) T \frac{\Omega}{4\pi}, \quad (14)$$

where T is the total observation time with two or more gravitational-wave detectors operating, and Ω is the field of view of the satellite’s GRB detector. Most of the S5-VSR1 GRBs were detected by *Swift*, with $\Omega = 1.4$ sr. The coincident observation time was approximately 1.3 yr. These give

$$\langle N_{\text{long}} \rangle \simeq 1 \times 10^{-6} \frac{R_{\text{long}}^{\text{obs}}}{0.5 \text{ Gpc}^{-3} \text{yr}^{-1}} \left(\frac{E_{\text{GW}}^{\text{iso}}}{0.01 M_{\odot}c^2} \right)^{3/2}. \quad (15)$$

Recent studies (Liang et al. 2007; Chapman et al. 2007) have indicated that there exists a local population of under-luminous long GRBs with an observed rate density approximately 10^3 times that of the high-luminosity population. For this population we have

$$\langle N_{\text{local}} \rangle \simeq 1 \times 10^{-3} \frac{R_{\text{local}}^{\text{obs}}}{500 \text{ Gpc}^{-3} \text{yr}^{-1}} \left(\frac{E_{\text{GW}}^{\text{iso}}}{0.01 M_{\odot}c^2} \right)^{3/2}. \quad (16)$$

For short GRBs the estimated local rate density is of order $R_{\text{short}}^{\text{obs}} \sim 10 \text{ Gpc}^{-3} \text{yr}^{-1}$ (Guetta & Piran 2006; Nakar et al. 2006). We therefore estimate the *a priori* expected number of short GRBs being observed during S5-VSR1 as

$$\langle N_{\text{short}} \rangle \simeq 2 \times 10^{-5} \frac{R_{\text{short}}^{\text{obs}}}{10 \text{ Gpc}^{-3} \text{yr}^{-1}} \left(\frac{E_{\text{GW}}^{\text{iso}}}{0.01 M_{\odot}c^2} \right)^{3/2}. \quad (17)$$

There is also evidence of a high-density local population of short GRBs (Nakar et al. 2006; Chapman et al. 2008), but these are thought to be due to extra-galactic SGRs, which are not so promising as GW sources.

It is clear that the detection of gravitational-wave emission associated with either a short or long GRB with the current LIGO-Virgo network is unlikely, though not impossible. Looking ahead, the enhanced LIGO and Virgo

detectors have recently begun their next data-taking run, S6-VSR2. Furthermore, the Fermi satellite is now operating, with a field of view of approximately $\Omega = 9.5$ sr. Assuming a similar observation time and sensitivity for S6-VSR2, the expected number of detections scales to

$$\langle N_{\text{long}} \rangle \simeq 7 \times 10^{-6} \quad (18)$$

$$\langle N_{\text{local}} \rangle \simeq 7 \times 10^{-3} \quad (19)$$

$$\langle N_{\text{short}} \rangle \simeq 1 \times 10^{-4}, \quad (20)$$

where we use the nominal values for R^{obs} , $E_{\text{GW}}^{\text{iso}}$ as in equations (15)–(17). Further in the future (c.2015), the planned advanced LIGO (Abbott et al. 2007) and advanced Virgo (Acernese et al. 2006) detectors will have amplitude sensitivities about an order of magnitude greater than the current detectors. Since the search volume scales as D^3 , there is a very good chance that we will be able to detect gravitational waves associated with one or more GRBs during an extended science run of the advanced detectors.

We are indebted to the observers of the electromagnetic events and the GCN for providing us with valuable data. The authors gratefully acknowledge the support of the United States National Science Foundation

for the construction and operation of the LIGO Laboratory, the Science and Technology Facilities Council of the United Kingdom, the Max-Planck-Society, and the State of Niedersachsen/Germany for support of the construction and operation of the GEO600 detector, and the Italian Istituto Nazionale di Fisica Nucleare and the French Centre National de la Recherche Scientifique for the construction and operation of the Virgo detector. The authors also gratefully acknowledge the support of the research by these agencies and by the Australian Research Council, the Council of Scientific and Industrial Research of India, the Istituto Nazionale di Fisica Nucleare of Italy, the Spanish Ministerio de Educación y Ciencia, the Conselleria d'Economia Hisenda i Innovació of the Govern de les Illes Balears, the Foundation for Fundamental Research on Matter supported by the Netherlands Organisation for Scientific Research, the Royal Society, the Scottish Funding Council, the Scottish Universities Physics Alliance, The National Aeronautics and Space Administration, the Carnegie Trust, the Leverhulme Trust, the David and Lucile Packard Foundation, the Research Corporation, and the Alfred P. Sloan Foundation. This document has been assigned LIGO Laboratory document number LIGO-P0900023-v13.

APPENDIX

GRB SAMPLE AND SEARCH RESULTS

Table 1 lists the 137 GRBs analyzed in this analysis, including the GRB name, time, sky position, and redshift (when known). In addition, for each GRB we display the results of the X-PIPELINE search for an associated GWB: the set of detectors used, the local probability of the loudest on-source event, and 90% confidence limits on the gravitational-wave amplitude and the distance to the progenitor. For approximately half of the GRBs there was no surviving event and hence no local probability. The limits are computed for circularly polarized 150 Hz and 1000 Hz sine-Gaussian waveforms. The distances are lower limits, assuming isotropic emission of $0.01 M_{\odot} c^2 = 1.8 \times 10^{53}$ erg of energy in gravitational waves. These limits include allowances for statistical and systematic errors as discussed in Sec. 6.2.

REFERENCES

- Abbott, B., et al. 2004, Nucl. Inst. & Meth. in Phys. Res., 517, 154
—, 2005, Phys. Rev. D, 72, 042002
—, 2007, <http://www.ligo.caltech.edu/docs/M/M060056-08/M060056-08.pdf>
—, 2008a, ApJ, 681, 1419
—, 2008b, Phys. Rev. D, 77, 062004
—, 2009a, Rep. Prog. Phys., 72, 076901
—, 2009b, arXiv:0905.0020
—, 2009c, in preparation
Acernese, F., et al. 2006, J. Phys.: Conf. Ser., 32, 223
—, 2007, Classical and Quantum Gravity, 24, S671
—, 2008a, Classical and Quantum Gravity, 25, 225001
—, 2008b, Classical and Quantum Gravity, 25, 114045
Anderson, W. G., Brady, P. R., Creighton, J. D. E., & Flanagan, E. E. 2001, Phys. Rev. D, 63, 042003
Astone, P., et al. 2002, Phys. Rev. D, 66, 102002
—, 2005, Phys. Rev. D, 71, 042001
Aylott, B., et al. 2009, Class. Quant. Grav., 26, 165008
Baiotti, L., Giacomazzo, B., & Rezzolla, L. 2008, Phys. Rev. D, 78, 084033
Berger, E., et al. 2005, ApJ, 634, 501
Biswas, R., Brady, P. R., Creighton, J. D. E., & Fairhurst, S. 2009, Classical and Quantum Gravity, 26, 175009 (19pp)
Blanchet, L. 2006, Living Reviews in Relativity, 9
Brady, P. R., Creighton, J. D. E., & Wiseman, A. G. 2004, Classical and Quantum Gravity, 21, S1775
Campana, S., et al. 2006, Nature, 442, 1008
Cannizzo, J. K., & Gehrels, N. 2009, ApJ, 700, 1047
Chapman, R., Priddey, R. S., & Tanvir, N. R. 2008, AIP Conf. Proc., 983, 304
Chapman, R., Tanvir, N. R., Priddey, R. S., & Levan, A. J. 2007, MNRAS, 382, L21
Chatterji, S., Blackburn, L., Martin, G., & Katsavounidis, E. 2004, Classical and Quantum Gravity, 21, S1809
Chatterji, S., Lazzarini, A., Stein, L., Sutton, P., Searle, A., & Tinto, M. 2006, Phys. Rev. D, 74, 082005
Davies, M. B., King, A., Rosswog, S., & Wynn, G. 2002, ApJ, 579, L63
Duncan, R. C., & Thompson, C. 1992, ApJ, 392, L9
Etienne, Z. B., et al. 2008, Phys. Rev. D, 77, 084002
Finn, L. S., Mohanty, S. D., & Romano, J. D. 1999, Phys. Rev. D, 60, 121101(R)
Flanagan, E. E., & Hughes, S. A. 1998, Phys. Rev. D, 57, 4566
Fox, D. B., et al. 2005, Nature, 437, 845
Fryer, C. L., Holz, D. E., & Hughes, S. A. 2002, ApJ, 565, 430
Fryer, C. L., Woosley, S. E., & Hartmann, D. H. 1999, ApJ, 526, 152
Galama, T. J., et al. 1998, Nature, 395, 670
GCN. 2007, <http://gcn.gsfc.nasa.gov/>
Gehrels, N., et al. 2004, ApJ, 611, 1005
Gehrels, N., et al. 2006, Nature, 444, 1044
Grote, H., et al. 2008, Classical and Quantum Gravity, 25, 114043
Guetta, D., & Piran, T. 2005, Astron. & Astrophys., 435, 421
—, 2006, Astron. & Astrophys., 453, 823
Gursel, Y., & Tinto, M. 1989, Phys. Rev. D, 40, 3884
Hjorth, J., et al. 2003, Nature, 423, 847

TABLE 1
GRB SAMPLE AND SEARCH RESULTS

GRB	z	UTC time	RA (deg)	Dec (deg)	network	p	150 Hz	1000 Hz	
							h_{rss}	D (Mpc)	h_{rss} D (Mpc)
051114‡	–	04:11:30	15 ^h 5 ^m 4 ^s	60°9′	H1H2	– (162)	7.98	5.7	29.9 0.229
051117	–	10:51:20	15 ^h 13 ^m 36 ^s	30°52′	H1H2	0.184 (250)	8.12	5.6	31.0 0.221
051117B	–	13:22:54	5 ^h 40 ^m 45 ^s	–19°17′	H1H2L1	– (57)	6.77	6.8	28.3 0.242
051210‡	–	05:46:21	22 ^h 0 ^m 47 ^s	–57°37′	H1H2	– (191)	6.60	6.9	27.0 0.254
051211‡	–	02:50:05.4	6 ^h 56 ^m 13 ^s	32°41′	H1H2L1	– (190)	4.83	9.5	21.2 0.324
051211B	–	22:05:44	23 ^h 2 ^m 45 ^s	55°5′	H1H2L1	– (105)	3.12	14.7	13.2 0.519
051213	–	07:13:04	16 ^h 48 ^m 19 ^s	–59°14′	H1H2L1	0.0769 (104)	2.62	17.5	11.3 0.609
051221B	–	20:03:20	20 ^h 49 ^m 26 ^s	53°2′	H1H2	– (82)	4.91	9.3	20.6 0.334
060102	–	21:17:28	21 ^h 55 ^m 20 ^s	–1°50′	H1H2	– (147)	6.84	6.7	27.8 0.247
060105	–	06:49:28	19 ^h 49 ^m 57 ^s	46°22′	H1H2L1	– (128)	5.44	8.4	23.6 0.291
060108	2.03	14:39:11.76	9 ^h 48 ^m 4 ^s	31°56′	H1H2L1	– (89)	4.92	9.3	20.4 0.336
060110	–	08:01:17	4 ^h 50 ^m 57 ^s	28°26′	H1H2L1	– (135)	3.58	12.8	15.5 0.444
060111	–	04:23:06	18 ^h 24 ^m 47 ^s	37°36′	H1H2L1	– (131)	4.97	9.2	21.1 0.325
060114	–	12:39:44	13 ^h 1 ^m 7 ^s	–4°45′	H1H2L1	– (118)	3.51	13.0	15.4 0.444
060115	3.53	13:08:00	3 ^h 36 ^m 1 ^s	17°20′	H1L1	– (117)	4.56	10.0	20.7 0.332
060116	6.6	08:37:27	5 ^h 38 ^m 48 ^s	–5°27′	H1H2L1	0.0402 (18000)	5.11	9.0	26.9 0.255
060121‡	–	22:24:54.5	9 ^h 9 ^m 57 ^s	45°40′	H1H2	– (159)	35.32	1.3	143.6 0.048
060202	–	08:40:55	2 ^h 23 ^m 17 ^s	38°23′	H1H2	– (207)	9.20	5.0	34.3 0.200
060203	–	23:55:35	6 ^h 54 ^m 0 ^s	71°50′	H1H2	– (174)	6.00	7.6	21.9 0.313
060206	4.045	04:46:53	13 ^h 31 ^m 44 ^s	35°3′	H1H2L1	0.444 (187)	4.94	9.3	21.9 0.313
060211B	–	15:55:15	5 ^h 0 ^m 18 ^s	14°57′	H1H2	– (149)	8.67	5.3	29.0 0.237
060223	4.41	06:04:23	3 ^h 40 ^m 45 ^s	–17°8′	H1H2L1	0.321 (162)	4.88	9.4	21.0 0.327
060306	–	00:49:10	2 ^h 44 ^m 23 ^s	–2°9′	H1H2L1	0.102 (186)	3.45	13.3	15.1 0.454
060312	–	01:36:12	3 ^h 3 ^m 6 ^s	12°49′	H1H2L1	– (196)	3.14	14.6	11.8 0.581
060313‡	<1.7	00:12:06	4 ^h 26 ^m 30 ^s	–10°52′	H1H2	– (186)	4.92	9.3	20.5 0.335
060319	–	00:55:42	11 ^h 45 ^m 28 ^s	60°2′	H1H2	– (187)	4.90	9.3	20.8 0.331
060323	–	14:32:36	11 ^h 37 ^m 39 ^s	50°0′	H1H2	– (84)	5.26	8.7	22.1 0.311
060403	–	13:12:17	18 ^h 49 ^m 21 ^s	8°20′	H1H2	– (207)	3.66	12.5	15.3 0.450
060418	1.49	03:06:08	15 ^h 45 ^m 43 ^s	–3°39′	H1H2L1	0.681 (141)	7.01	6.5	34.1 0.201
060427	–	11:43:10	8 ^h 16 ^m 42 ^s	62°39′	H1H2L1	– (168)	4.60	9.9	20.5 0.334
060427B‡	–	23:51:55	6 ^h 33 ^m 53 ^s	21°21′	H1H2L1	0.228 (114)	2.44	18.7	10.6 0.649
060428	–	03:22:48	8 ^h 14 ^m 8 ^s	–37°10′	H1H2	– (207)	18.52	2.5	79.7 0.086
060428B	–	08:54:38	15 ^h 41 ^m 31 ^s	62°2′	H1H2L1	0.0139 (18000)	2.39	19.2	10.8 0.637
060429‡	–	12:19:51.00	7 ^h 42 ^m 3 ^s	–24°57′	H1H2	– (166)	3.36	13.6	14.5 0.472
060501	–	08:14:58	21 ^h 53 ^m 32 ^s	43°60′	H1H2	– (172)	5.72	8.0	24.0 0.286
060510	–	07:43:27	6 ^h 23 ^m 25 ^s	–1°10′	H1H2L1	– (114)	3.36	13.6	15.1 0.455
060510B	4.9	08:22:14	15 ^h 56 ^m 52 ^s	78°36′	H1H2L1	0.0124 (18000)	2.89	15.9	14.7 0.466
060515	–	02:27:52	8 ^h 29 ^m 11 ^s	73°34′	H1H2L1	0.509 (57)	2.36	19.4	10.6 0.650
060516	–	06:43:34	4 ^h 44 ^m 40 ^s	–18°6′	H1H2L1	0.221 (140)	2.09	21.9	10.4 0.657
060526	3.21	16:28:30	15 ^h 31 ^m 21 ^s	0°18′	H1H2L1	0.731 (52)	2.56	17.9	11.7 0.587
060605	3.8	18:15:44	21 ^h 28 ^m 38 ^s	–6°3′	H1H2	– (201)	10.63	4.3	43.3 0.158
060607	–	05:12:13	21 ^h 58 ^m 51 ^s	–22°30′	H1H2L1	0.0945 (201)	4.88	9.4	21.9 0.314
060607B	–	23:32:44	2 ^h 48 ^m 12 ^s	14°45′	H1H2L1	– (135)	9.49	4.8	41.2 0.167
060614	0.125	12:43:48	21 ^h 23 ^m 31 ^s	–53°2′	H2L1	– (61)	26.59	1.7	118.8 0.058
060707	3.43	21:30:19	23 ^h 48 ^m 18 ^s	–17°54′	H1H2L1	– (188)	2.53	18.1	11.2 0.612
060712	–	21:07:43	12 ^h 16 ^m 16 ^s	35°32′	H1H2	– (65)	4.89	9.4	19.9 0.344
060714	2.71	15:12:00	15 ^h 11 ^m 25 ^s	–6°33′	H1H2	– (162)	3.88	11.8	15.6 0.440
060719	–	06:50:36	1 ^h 13 ^m 40 ^s	–48°23′	H1H2L1	– (127)	3.46	13.2	15.3 0.447
060804	–	07:28:19	7 ^h 28 ^m 52 ^s	–27°14′	H1H2L1	– (109)	2.34	19.5	10.8 0.635
060805	–	04:47:49	14 ^h 43 ^m 42 ^s	12°35′	H1H2L1	0.569 (195)	3.34	13.7	14.9 0.462
060807	–	14:41:35	16 ^h 50 ^m 1 ^s	31°36′	H1H2L1	0.00967 (18000)	4.70	9.7	21.2 0.323
060813	–	22:50:22	7 ^h 27 ^m 34 ^s	–29°51′	H1H2L1	0.297 (185)	3.49	13.1	15.8 0.434
060814	0.84	23:02:19	14 ^h 45 ^m 21 ^s	20°36′	H2L1	0.0741 (135)	3.21	14.2	13.5 0.507
060825	–	02:59:57	1 ^h 12 ^m 31 ^s	55°48′	H1H2	– (163)	5.06	9.1	21.9 0.313
060904	–	01:03:21	15 ^h 50 ^m 55 ^s	44°59′	H1H2L1	– (146)	1.82	25.1	8.1 0.843
060904B	0.703	02:31:03	3 ^h 52 ^m 52 ^s	0°44′	H1H2	0.391 (179)	3.57	12.8	15.3 0.447
060906	3.685	08:32:46	2 ^h 42 ^m 50 ^s	30°21′	H1H2L1	– (187)	2.30	19.9	10.6 0.647
060908	2.43	08:57:22	2 ^h 7 ^m 17 ^s	0°20′	H1H2L1	0.487 (189)	2.34	19.6	10.9 0.631
060919	–	07:48:38	18 ^h 27 ^m 36 ^s	–50°60′	H1H2L1	0.130 (138)	3.26	14.0	15.1 0.456
060923	–	05:12:15	16 ^h 58 ^m 30 ^s	12°20′	H1H2	– (142)	5.11	9.0	22.3 0.308
060923C	–	13:33:02	23 ^h 4 ^m 29 ^s	3°57′	H1H2	– (199)	37.92	1.2	164.5 0.042
060927	5.6	14:07:35	21 ^h 58 ^m 11 ^s	5°22′	H1H2	0.576 (184)	4.79	9.6	21.1 0.325
060928	–	01:17:01.00	8 ^h 30 ^m 27 ^s	–42°44′	H1H2	0.228 (114)	2.96	15.5	11.7 0.587

TABLE 1
– *Continued*

GRB	z	UTC time	RA (deg)	Dec (deg)	network	p	150 Hz		1000 Hz	
							h_{RSS}	D (Mpc)	h_{RSS}	D (Mpc)
060930	–	09:04:09	20 ^h 18 ^m 9 ^s	–23°38′	H1L1	0.0248 (18000)	6.95	6.6	36.9	0.186
061002	–	01:03:29	14 ^h 41 ^m 25 ^s	48°44′	H1H2L1	– (193)	2.49	18.3	11.2	0.615
061006‡	–	16:45:50	7 ^h 23 ^m 60 ^s	–79°12′	H1H2	0.310 (184)	3.61	12.7	18.8	0.365
061007	1.261	10:08:08	3 ^h 5 ^m 12 ^s	–50°30′	H1H2L1	0.775 (160)	9.70	4.7	42.7	0.161
061021	<2.0	15:39:07	9 ^h 40 ^m 35 ^s	–21°57′	H1H2L1	0.979 (94)	4.32	10.6	19.8	0.347
061027	–	10:15:02	18 ^h 3 ^m 58 ^s	–82°14′	H1H2	– (193)	4.42	10.4	15.4	0.446
061102	–	01:00:31	9 ^h 53 ^m 34 ^s	–17°0′	H1H2L1	– (113)	2.38	19.2	10.7	0.639
061110	0.757	11:47:21	22 ^h 25 ^m 8 ^s	–2°15′	H1H2L1	0.214 (168)	3.12	14.6	14.1	0.486
061122	–	07:56:49	20 ^h 15 ^m 21 ^s	15°31′	H1H2L1	0.575 (73)	4.36	10.5	20.6	0.334
061126	<1.5	08:47:56	5 ^h 46 ^m 28 ^s	64°12′	H1H2	– (144)	2.79	16.4	11.0	0.622
061201‡	–	15:58:36	22 ^h 8 ^m 19 ^s	–74°34′	H1H2	0.0222 (18000)	3.53	13.0	16.8	0.408
061217‡	0.827	03:40:08	10 ^h 41 ^m 40 ^s	–21°8′	H1L1	– (187)	3.32	13.8	15.8	0.433
061218	–	04:05:05	9 ^h 56 ^m 57 ^s	–35°13′	H1H2L1	– (169)	3.67	12.5	15.9	0.431
061222	–	03:28:52	23 ^h 53 ^m 2 ^s	46°32′	H1H2	– (207)	4.85	9.4	15.9	0.430
061222B	3.355	04:11:02	7 ^h 1 ^m 24 ^s	–25°52′	H1H2L1	0.444 (180)	6.50	7.0	28.0	0.245
070103	–	20:46:39.41	23 ^h 30 ^m 20 ^s	26°49′	H1H2	– (207)	5.37	8.5	21.4	0.321
070107	–	12:05:18	10 ^h 37 ^m 41 ^s	–53°12′	H1H2L1	– (186)	15.57	2.9	60.2	0.114
070110	2.352	07:22:41	0 ^h 3 ^m 44 ^s	–52°59′	H1H2L1	0.609 (207)	2.50	18.3	11.1	0.618
070129	–	23:35:10	2 ^h 28 ^m 0 ^s	11°44′	H1H2	0.261 (207)	3.50	13.1	14.8	0.462
070201‡	–	15:23:10.78	0 ^h 44 ^m 21 ^s	42°18′	H1H2	0.0791 (177)	6.38	7.2	27.8	0.247
070208	1.165	09:10:34	13 ^h 11 ^m 35 ^s	61°57′	H1H2L1	0.0847 (177)	1.87	24.5	10.4	0.658
070209‡	–	03:33:41	3 ^h 4 ^m 51 ^s	–47°23′	H1H2L1	0.605 (185)	11.24	4.1	52.6	0.131
070219	–	01:10:16	17 ^h 20 ^m 53 ^s	69°21′	H1L1	0.192 (104)	3.61	12.7	20.6	0.334
070223	–	01:15:00	10 ^h 13 ^m 49 ^s	43°8′	H1H2L1	0.219 (137)	3.36	13.6	15.3	0.448
070309	–	10:01:03	17 ^h 34 ^m 44 ^s	–37°57′	H1H2L1	0.357 (196)	3.92	11.7	18.6	0.370
070311	–	01:52:35	5 ^h 50 ^m 10 ^s	3°23′	H1H2L1	0.447 (188)	2.35	19.5	10.9	0.631
070318	0.836	07:28:56	3 ^h 13 ^m 57 ^s	–42°57′	H1H2L1	0.873 (166)	2.14	21.4	10.1	0.680
070330	–	22:51:31	17 ^h 58 ^m 8 ^s	–63°48′	H1H2L1	0.134 (201)	1.87	24.5	10.2	0.671
070402	–	15:48:35.00	20 ^h 44 ^m 44 ^s	27°24′	H1H2L1	0.299 (87)	2.24	20.5	10.3	0.667
070411	2.954	20:12:33	7 ^h 9 ^m 23 ^s	1°3′	H2L1	0.0733 (150)	18.35	2.5	75.3	0.091
070412	–	01:27:03	12 ^h 6 ^m 6 ^s	40°8′	H1H2L1	0.915 (177)	2.49	18.4	11.1	0.621
070419	0.97	09:59:26	12 ^h 11 ^m 1 ^s	39°54′	H1H2L1	0.715 (123)	2.75	16.6	12.8	0.535
070419B	–	10:44:05	21 ^h 2 ^m 50 ^s	–31°16′	H1H2	– (193)	6.14	7.4	24.9	0.276
070420	–	06:18:13	8 ^h 4 ^m 59 ^s	–45°34′	H1H2L1	0.805 (133)	3.58	12.8	18.8	0.365
070427	–	08:31:08	1 ^h 55 ^m 29 ^s	–27°36′	H1H2L1	– (150)	2.02	22.6	10.1	0.679
070429	–	01:35:10	19 ^h 50 ^m 47 ^s	–32°25′	H1L1	– (152)	1.79	25.6	10.6	0.647
070429B‡	–	03:09:04	21 ^h 52 ^m 1 ^s	–38°51′	H1H2L1	0.443 (194)	1.75	26.2	8.0	0.862
070506	2.31	05:35:58	23 ^h 8 ^m 49 ^s	10°43′	H1H2L1	0.811 (122)	3.17	14.4	15.3	0.450
070508	<2.3	04:18:17	20 ^h 51 ^m 20 ^s	–78°23′	H1H2L1	0.147 (184)	2.37	19.3	10.7	0.642
070518	–	14:26:21	16 ^h 56 ^m 53 ^s	55°17′	H1H2	0.525 (120)	3.48	13.1	15.1	0.453
070520	–	13:05:10	12 ^h 53 ^m 1 ^s	75°0′	H1H2V1	– (180)	4.20	10.9	16.2	0.424
070520B	–	17:44:53	8 ^h 7 ^m 33 ^s	57°35′	L1V1	0.487 (195)	22.37	2.0	30.0	0.229
070521	–	06:51:10	16 ^h 10 ^m 38 ^s	30°16′	H1H2V1	– (167)	2.62	17.5	12.1	0.569
070529	2.4996	12:48:28	18 ^h 54 ^m 54 ^s	20°39′	H1H2L1V1	0.0776 (18000)	2.86	16.0	13.0	0.528
070531	–	02:10:17	0 ^h 26 ^m 53 ^s	74°19′	L1V1	0.533 (184)	11.47	4.0	18.4	0.372
070611	2.04	01:57:13	0 ^h 8 ^m 1 ^s	–29°45′	H1H2L1	– (172)	1.80	25.4	8.5	0.805
070612	0.617	02:38:45	8 ^h 5 ^m 25 ^s	37°15′	L1V1	0.174 (207)	13.85	3.3	68.3	0.100
070612B	–	06:21:17	17 ^h 26 ^m 52 ^s	–8°45′	H1H2L1V1	0.129 (124)	2.62	17.5	14.4	0.477
070615	–	02:20:35	2 ^h 57 ^m 14 ^s	–4°24′	H1H2L1V1	0.219 (169)	2.57	17.8	11.2	0.614
070616	–	16:29:33	2 ^h 8 ^m 23 ^s	56°57′	H1H2V1	0.633 (166)	2.79	16.4	10.8	0.636
070621	–	23:17:39	21 ^h 35 ^m 13 ^s	–24°49′	H1L1V1	0.652 (69)	1.79	25.6	10.0	0.689
070626	–	04:05:33	9 ^h 25 ^m 25 ^s	–39°52′	H1L1V1	– (86)	4.96	9.2	18.6	0.368
070628	–	14:41:02	7 ^h 41 ^m 5 ^s	–20°17′	H1V1	0.767 (133)	9.88	4.6	43.7	0.157
070704	–	20:05:57	23 ^h 38 ^m 50 ^s	66°15′	H1H2L1	0.237 (80)	3.66	12.5	15.1	0.455
070707‡	–	16:08:38	17 ^h 51 ^m 0 ^s	–68°53′	L1V1	0.799 (184)	36.04	1.3	85.5	0.080
070714‡	–	03:20:31	2 ^h 51 ^m 44 ^s	30°14′	H1H2L1V1	– (114)	5.04	9.1	26.0	0.264
070714B‡	0.92	04:59:29	3 ^h 51 ^m 25 ^s	28°18′	H1H2L1V1	0.965 (141)	5.46	8.4	20.7	0.331
070721	–	10:01:08	0 ^h 12 ^m 35 ^s	–28°32′	H1H2L1V1	– (138)	4.29	10.7	15.2	0.450
070721B	3.626	10:33:48	2 ^h 12 ^m 31 ^s	–2°12′	H1H2L1V1	0.492 (118)	3.49	13.1	15.3	0.450
070724‡	0.457	10:53:50	1 ^h 51 ^m 18 ^s	–18°37′	H1H2L1V1	0.191 (110)	4.76	9.6	19.2	0.357
070724B	–	23:25:09	1 ^h 10 ^m 31 ^s	57°40′	H1H2L1V1	– (164)	4.85	9.4	19.9	0.344
070729‡	–	00:25:53	3 ^h 45 ^m 11 ^s	–39°20′	H1H2L1V1	– (155)	2.33	19.6	10.7	0.639
070731	–	09:33:22	21 ^h 54 ^m 19 ^s	–15°44′	H1H2L1V1	– (84)	4.97	9.2	16.7	0.410

TABLE 1
– *Continued*

GRB	z	UTC time	RA (deg)	Dec (deg)	network	p	150 Hz		1000 Hz	
							h_{rss}	D (Mpc)	h_{rss}	D (Mpc)
070802	2.45	07:07:25	2 ^h 27 ^m 37 ^s	−55°31′	H1H2	– (161)	3.56	12.8	15.4	0.445
070805	–	19:55:45	16 ^h 20 ^m 14 ^s	−59°57′	H1H2L1	0.193 (207)	2.51	18.2	13.9	0.493
070809‡	–	19:22:17	13 ^h 35 ^m 4 ^s	−22°7′	H1H2V1	– (183)	9.20	5.0	38.6	0.178
070810	2.17	02:11:52	12 ^h 39 ^m 47 ^s	10°45′	H1H2L1V1	– (120)	4.48	10.2	15.4	0.446
070810B‡	–	15:19:17	0 ^h 35 ^m 48 ^s	8°49′	H1H2L1	0.239 (180)	4.80	9.5	21.4	0.321
070821	–	12:49:24.00	6 ^h 22 ^m 6 ^s	−63°51′	H1H2L1V1	0.303 (119)	3.96	11.6	14.7	0.467
070911	–	05:57:44	1 ^h 43 ^m 17 ^s	−33°29′	H1H2L1V1	0.512 (160)	4.74	9.6	17.7	0.387
070917	–	07:33:56	19 ^h 35 ^m 42 ^s	2°25′	H1H2V1	0.295 (193)	4.23	10.8	15.6	0.439
070920	–	04:00:13	6 ^h 43 ^m 52 ^s	72°15′	H1H2L1V1	– (123)	3.54	12.9	15.6	0.441
070920B	–	21:04:32	0 ^h 0 ^m 30 ^s	−34°51′	H1H2L1V1	0.600 (60)	2.26	20.2	10.4	0.659
070923‡	–	19:15:23	12 ^h 18 ^m 30 ^s	−38°18′	H1H2L1	– (196)	4.91	9.3	26.0	0.264

NOTE. — Information and limits on associated GWB emission for each of the GRBs studied. The first five columns are GRB name, redshift (if known), time, and sky position (right ascension and declination). The remaining columns display the results of the X-PIPELINE search for an associated GWB: the set of detectors used, the local probability p of the loudest on-source event, and 90% confidence limits on the gravitational-wave amplitude and the distance to the progenitor. A p value of “–” indicates no event survived all cuts. The number in parentheses after the p value is the number of off-source segments used to estimate p . The limits are computed for circularly polarized 150 Hz and 1000 Hz sine-Gaussian waveforms. The h_{rss} amplitudes are in units of $10^{-22} \text{ Hz}^{-1/2}$. The distances are lower limits, assuming isotropic emission of $E_{\text{GW}}^{\text{iso}} = 0.01 M_{\odot} c^2 = 1.8 \times 10^{52} \text{ erg}$ in gravitational waves, and scale as $D \propto (E_{\text{GW}}^{\text{iso}})^{1/2}$. These limits include allowances for systematics as discussed in Sec. 6.2. A double dagger (§) following the GRB name indicates that it was also included in the template-based search for binary inspiral gravitational-wave signals presented in Abbott et al. (2009c).

- Hurley, K., et al. 2009, in American Institute of Physics Conference Series, Vol. 1133, GAMMA-RAY BURST: Sixth Huntsville Symposium, ed. C. Meegan, C. Kouveliotou, & N. Gehrels, 55–57
- Isaacson, R. A. 1968, Phys. Rev., 166, 1272
- Iwamoto, K., et al. 1998, Nature, 395, 672
- King, A., O’Brien, P. T., Goad, M. R., Osborne, J., Olsson, E., & Page, K. 2005, ApJ, 630, L113
- Klimenko, S., Mohanty, S., Rakhmanov, M., & Mitselmakher, G. 2005, Phys. Rev. D, 72, 122002
- . 2006, J. Phys. Conf. Ser., 32, 12
- Kobayashi, S., & Meszaros, P. 2003, ApJ, 585, L89
- Kouveliotou, C., Meegan, C. A., Fishman, G. J., Bhat, N. P., Briggs, M. S., Koshut, T. M., Paciesas, W. S., & Pendleton, G. N. 1993, ApJ, 413, L101
- Kulkarni, S. R., et al. 1998, Nature, 395, 663
- Le, T., & Dermer, C. D. 2007, ApJ, 661, 394
- Leonor, I., Frey, R., Jones, G., Marka, S., Marka, Z., & Sutton, P. J. 2009, Classical and Quantum Gravity, in press
- Liang, E., Zhang, B., Virgili, F., & Dai, Z. G. 2007, ApJ, 662, 1111
- Malesani, D., et al. 2004, ApJ, 609, L5
- Mazets, E. P., et al. 2008, ApJ, 680, 545
- Mészáros, P. 2006, Rept. Prog. Phys., 69, 2259
- Mirabal, N., Halpern, J. P., An, D., Thorstensen, J. R., & Terndrup, D. M. 2006, ApJ, 643, L99
- Mohanty, S., Rakhmanov, M., Klimenko, S., & Mitselmakher, G. 2006, Classical and Quantum Gravity, 23, 4799
- Nakar, E. 2007, Physics Reports, 442, 166
- Nakar, E., Gal-Yam, A., & Fox, D. B. 2006, ApJ, 650, 281
- Ott, C. D. 2009, Classical and Quantum Gravity, 26, 063001
- Piro, A. L., & Pfahl, E. 2007, ApJ, 658, 1173
- Price, P. A., Berger, E., & Fox, D. B. 2006, GRB Coordinates Network, 5275, 1
- Rakhmanov, M. 2006, Classical and Quantum Gravity, 23, S673
- Ricker, G. R., et al. 2003, in American Institute of Physics Conference Series, Vol. 662, Gamma-Ray Burst and Afterglow Astronomy 2001: A Workshop Celebrating the First Year of the HETE Mission, ed. G. R. Ricker & R. K. Vanderspek, 3–16
- Schmidt, M. 2001, ApJ, 552, 36
- Sokolov, V. V. 2001, BSAO, 51, 38
- Summerscales, T. Z., Burrows, A., Finn, L. S., & Ott, C. D. 2008, ApJ, 678, 1142
- Sutton, P. J., et al. 2009, arXiv:0908.3665
- Sylvestre, J. 2002, Phys. Rev. D, 66, 102004
- van Putten, M. H., et al. 2004, Phys. Rev. D, 69, 044007
- Winkler, C., et al. 2003, Astron. & Astrophys., 411, L1
- Wright, E. L. 2006, PASP, 118, 1711